lncMIR155HG/miR-212-3p/HMGA2 axis contributes to chondrocyte injury and potential mTOR-related autophagy dysregulation in osteoarthritis

FU SHEN[1*], YEXIAO TANG[2*], LISHENG CUI[1], RUI PENG[2], YAWEN DENG[1], XINYU ZHENG[1], RONG DENG[1], XIAOTONG XU[3] and SHUNDE CHEN[1]

[1]Department of Orthopedics, Yongzhou Hospital of Traditional Chinese Medicine, Yongzhou, Hunan 425000, P.R. China; [2]Department of Internal Medicine, Yongzhou Hospital of Traditional Chinese Medicine, Yongzhou, Hunan 425000, P.R. China; [3]Department of Orthopedic Surgery, The First Hospital of Hunan University of Chinese Medicine, Changsha, Hunan 410007, P.R. China

Received June 10, 2026; Accepted October 14, 2026

DOI: 10.3892/etm.2026.13363

Abstract. Osteoarthritis (OA) is a common degenerative joint disease characterized by progressive cartilage deterioration and chondrocyte injury. Despite long non-coding RNAs having been increasingly recognized as important regulators of chondrocyte homeostasis, the role of long non-coding RNA MIR155HG in OA-related chondrocyte injury and autophagy-associated signaling remains unclear. The present study analyzed public Gene Expression Omnibus datasets to identify high mobility group AT-hook 2 (HMGA2)-associated regulatory networks in OA. Bioinformatics prediction, support vector machine analysis and co-expression modeling were used to construct a candidate MIR155HG/miR-212-3p/HMGA2 competitive endogenous RNA regulatory axis. In IL-1β-induced human immortalized chondrocytes, MIR155HG knockdown attenuated apoptosis, reactive oxygen species accumulation, mitochondrial membrane potential loss and mitochondrial ultrastructural damage. MIR155HG knockdown also decreased MMP13 expression and increased type II collagen α 1 chain expression, suggesting a reduction in extracellular matrix degradation. Dual-luciferase reporter assays further determined interactions between miR-212-3p and MIR155HG, as well as between miR-212-3p and HMGA2. Rescue experiments revealed that miR-212-3p inhibition partially counteracted the effects of MIR155HG knockdown on chondrocyte injury, HMGA2 expression and mTOR-associated autophagy signaling. The present findings suggested that MIR155HG may participate in IL-1β-induced chondrocyte injury through the miR-212-3p/HMGA2 axis and may be associated with mTOR-related autophagy dysregulation in OA.

Correspondence to: Dr Xiaotong Xu, Department of Orthopedic Surgery, The First Hospital of Hunan University of Chinese Medicine, 95 Shaoshan Middle Road, Yuhua, Changsha, Hunan 410007, P.R. China
E-mail: xxtong33@hnucm.edu.cn

Dr Shunde Chen, Department of Orthopedics, Yongzhou Hospital of Traditional Chinese Medicine, 14 Jiuyi Lane, Lengshuitan, Yongzhou, Hunan 425000, P.R. China
E-mail: 992691017@qq.com

*Contributed equally

Key words: osteoarthritis, long non-coding RNA MIR155HG, microRNA-212-3p, high mobility group AT-hook 2, mTOR signaling, autophagy, chondrocyte injury

Introduction

Osteoarthritis (OA), the most prevalent joint disorder, is characterized by the progressive degeneration of articular cartilage (1). OA is the leading cause of disability among the elderly, affecting ~12% of the aging population (2,3). The global prevalence of OA has surpassed 300 million individuals, with an annual increase in its incidence rate being reported (4). OA has emerged as a notable health issue. The pathogenesis of OA is complex and apoptosis of articular chondrocytes serves a key role in its progression (5). Evidence has indicated that mechanical stress, age-related changes and obesity-associated factors contribute to the pathological increase in pro-inflammatory cytokines, particularly IL-1β. This cytokine elevation stimulates the expression of downstream inflammatory mediators, including MMPs, cyclooxygenase-2 and inducible nitric oxide synthase, ultimately leading to chondrocyte loss and extracellular matrix degradation (6,7). Mitochondrial dysfunction is also involved in chondrocyte degeneration. Mitochondria are the primary source of cellular ATP and the central regulators of redox homeostasis in chondrocytes. Under pathological stimuli such as IL-1β, mechanical overload and oxidative stress, chondrocyte mitochondria exhibit structural and functional abnormalities, including loss of mitochondrial membrane potential, impaired oxidative phosphorylation and excessive accumulation of mitochondrial reactive oxygen species (mtROS). Excessive mtROS not only damages mitochondrial DNA, proteins and lipids, but also triggers opening of the mitochondrial permeability transition pore, release of cytochrome *c* into the cytosol and subsequent activation of

the caspase-9/caspase-3 cascade, thereby driving chondrocyte apoptosis (8,9). Chondrocytes are the only cells in cartilage tissue, exhibiting low resistance to apoptosis and necrosis, as well as being prone to large-scale cell death (10). Currently, there is a paucity of non-surgical treatment options for OA. Despite medications, including diclofenac, glucosamine and nonsteroidal anti-inflammatory drugs, being used to alleviate symptoms in patients with early-stage OA, those with advanced OA often require arthroplasty. Therefore, investigating OA pathogenesis and enhancing chondrocyte survival rate may be pivotal in developing effective treatments for OA (11,12).

Apoptosis, a gene-regulated cell death process, is key in embryonic development and fetal organ formation (13). It also serves a role in pathological damage, with chondrocyte apoptosis being important for OA progression (14). Autophagy, a conserved mechanism that removes damaged organelles and proteins through the autophagosome-lysosome pathway, is central to cellular balance and preventing disease (15,16). Studies have indicated a close association between autophagy and apoptosis, both influencing OA pathogenesis (17-19). In OA development, autophagy protects chondrocytes from apoptosis and maintains cellular homeostasis by removing damaged proteins and organelles. It also enhances chondrocyte function and cartilage development (20,21). Dysfunctional autophagy is also associated with OA progression and severity as activating autophagy and reducing apoptosis can inhibit OA development. In a rat OA model, sirtuin 3 overexpression was shown to inhibit the PI3K/Akt/mTOR pathway, reduce apoptosis, activate autophagy and improve joint injury. These findings suggest that promoting autophagy could help prevent OA (22).

Long non-coding RNAs (lncRNAs) are transcripts >200 nucleotides long that do not code for proteins; however, they serve roles in gene regulation (23,24) and are involved in chromatin remodeling, cell proliferation and apoptosis (25,26). In OA, lncRNA expression patterns change. Zhou *et al* (27) analyzed lncRNA expression profiles of 185 patients with OA and 76 healthy controls from the GEO database and found that lncRNA MIR155HG was significantly upregulated in patients with OA. This finding was subsequently validated in peripheral blood samples collected from an independent cohort of 30 patients with OA and 15 healthy controls. These results suggest that lncRNA MIR155HG may serve as a potential molecular biomarker for the clinical diagnosis of OA. lncRNA MIR155HG is important in cartilage physiology, as it is induced in chondrocyte progenitor cells under high pressure (28). It regulates autophagy and apoptosis, with increased expression in mice with spinal cord injury. Silencing reduces neuronal apoptosis, enhances autophagy and improves glial scar formation and motor function (29). However, to the best of our knowledge, its role in OA progression and the potential benefits of silencing it to activate autophagy in OA remain unexplored.

lncRNAs can act as competitive endogenous RNAs by binding to miRNAs, reducing their inhibitory effects on target genes and affecting disease progression (30). High mobility group AT-hook 2 (HMGA2) is a transcription factor involved in angiogenesis, tumor metastasis, stem cell self-renewal and cartilage damage in OA (31,32). HMGA2 expression is associated with OA severity and its upregulation has been observed in arthritis mice models (33,34). MiR-let-7a, which targets HMGA2, has been shown to improve joint injury in OA mice (35). Numerous studies have reported an association between HMGA2 and autophagy, with elevated HMGA2 expression in retinal ischemic injury sites having promoted apoptosis and neuroinflammation. In HMGA2 knockout mice, autophagy-related protein expression has been shown to increase, thus reducing retinal neuron apoptosis (36,37). However, the role of HMGA2 in OA remains unclear.

The present bioinformatics analysis indicated that HMGA2 expression was elevated in the analyzed OA dataset and was associated with mTOR-related signaling and autophagy-associated pathways. Using a support vector machine (SVM) algorithm, MIR155HG and miR-212-3p were identified as potential regulators of HMGA2. To test the hypothesis, human immortalized chondrocytes were stimulated with IL-1β to create an *in vitro* OA model. MIR155HG antisense oligonucleotides were used to knock down its function, allowing the present study to investigate how MIR155HG affects chondrocyte apoptosis and autophagy. Overall, the present study examined the MIR155HG/miR-212-3p/HMGA2 axis and its potential impact on the mTOR signaling pathway, aiming to provide new insights into chondrocyte homeostasis in OA.

Materials and methods

Experimental cells and culture conditions. The human immortalized chondrocyte cell line iCell-0092a and its specialized culture medium iCell-0092a-001b were bought from Cellverse Bioscience Technology Co., Ltd. The 293T cell line (cat. no. CL-0005) was obtained from Procell Life Science & Technology Co., Ltd. Cells were maintained in a humidified incubator at 37˚C with 5% CO_2. The culture medium was replaced every 2-3 days and the cells were passaged using 0.25% trypsin when they reached ~80-90% confluence. Both cell lines were commercially obtained established cell lines and no primary patient-derived cells were used in the present study. The immortalized chondrocyte cell line iCell-0092a was not newly isolated from a patient by the present research group and was purchased as an established experimental cell line. The passage number dating back to the original establishment of the commercial cell lines was not provided by the suppliers and therefore could not be reliably traced. After thawing and recovery from the supplier-provided frozen vials, cells were used within 3-5 passages.

Establishment of the IL-1β-induced chondrocyte injury model and cell transfection. To establish an *in vitro* OA-like chondrocyte injury model, 3-5x10^5 immortalized chondrocytes were seeded into culture plates and stimulated with recombinant human IL-1β (20 ng/ml; cat. no. CG-93, Novoprotein Scientific Inc.) at 37˚C for 48 h. For MIR155HG knockdown, cells were transfected with 12.5 μl of MIR155HG-targeting antisense oligonucleotides (ASO-MIR155HG) or the corresponding negative control oligonucleotides (ASO-NC) using Lipofectamine® 3000 (Invitrogen; Thermo Fisher Scientific, Inc.), following the manufacturer's instructions (oligonucleotide dry powder dissolved in DEPC water: 125 μl/1OD). ASO-MIR155HG and ASO-NC were synthesized by General Bio (Anhui) Co., Ltd. Specific sequence information is shown in Table I. To examine whether miR-212-3p participated in

Table I. lncMIR155HG ASO interference sequences.

ASO name	ASO sequence (5'-3')
lncMIR155HG-ASO-1-417	(mU)*(mA)*(mU)*(mC)*(mC)*A*G*C*A*G*G*G*T*G*A*(mU)*(mC)*(mA)*(mU)
lncMIR155HG-ASO-2-1076	(mU)*(mU)*(mC)*(mU)*(mC)*T*G*C*T*C*G*C*A*C*A*(mA)*(mC)*(mC)*(mG)*(mU)
lncMIR155HG-ASO-3-748	(mA)*(mA)*(mC)*(mU)*(mG)*G*A*G*G*T*T*A*G*T*A*(mG)*(mU)*(mC)*(mC)*(mU)
ASO-NC	C*C*T*T*CCCTGAAGGTTC*C*T*C*C

lnc, long non-coding RNA; ASO, antisense oligonucleotides; MIR, microRNA; NC, negative control.

the regulatory effects of MIR155HG, miR-212-3p inhibitor or inhibitor NC was transfected alone or in combination with ASO-MIR155HG. At 48 h post-transfection, IL-1β was stimulated for 48 h, and chondrocytes were harvested for reverse transcription-quantitative PCR (RT-qPCR), flow cytometry, transmission electron microscopy, immunofluorescence staining and western blotting. A dual-luciferase reporter assay was performed separately in 293T cells to validate the predicted binding associations among MIR155HG, miR-212-3p and HMGA2. The cells were divided into the following groups: i) Control; ii) Model; iii) Model + ASO-NC; and iv) Model + ASO-MIR155HG. For the rescue experiments, the cells were divided into four groups: i) Model + inhibitor NC + ASO-NC; ii) Model + inhibitor NC + ASO-MIR155HG; iii) Model + miR-212-3p inhibitor + ASO-NC; and iv) Model + miR-212-3p inhibitor + ASO-MIR155HG.

Reagents and antibodies. Specialized immortalized human chondrocyte medium was obtained from Cellverse Bioscience Technology Co., Ltd. FBS was obtained from Gibco (Thermo Fisher Scientific, Inc.). Recombinant human IL-1β was acquired from Novoprotein Scientific Inc. Lipofectamine® 3000 and OPTI-MEM were obtained from Invitrogen and Gibco (Thermo Fisher Scientific, Inc.), respectively. The Dual-Luciferase Reporter Gene Assay Kit was obtained from Beyotime Biotechnology. The reactive oxygen species (ROS) Assay Kit (cat. no. KGT010-1, 100 assays; KeyGEN BioTECH Co., Ltd.), Annexin V-FITC/PI Apoptosis Detection Kit [cat. no. AP101-100; MultiSciences (Lianke) Biotech Co., Ltd.] and JC-1 Mitochondrial Membrane Potential Assay Kit (cat. no. BB-4105; BestBio Science Co., Ltd.) were used to assess cellular injury-related phenotypes. For molecular assays, Trizon reagent (cat. no. CW0580S; CWBIO/CoWin Biosciences), RT reagents (cat. no. R223-01; Vazyme Biotech Co., Ltd.), qPCR reagents (cat. no. CW3360M; CWBIO/CoWin Biosciences), RIPA lysis buffer (cat. no. C1053; Beijing Applygen Technologies Inc.), BCA protein assay kit (cat. no. E-BC-K318-M; Elabscience Biotechnology Co., Ltd.), PVDF membranes (cat. no. IPVH00010; Merck Millipore) and ECL detection reagents (cat. no. RJ239676; Thermo Fisher Scientific, Inc.) were used following the manufacturers' instructions. Primary antibodies against MMP13, type II collagen α 1 chain (COL2A1), mTOR, phosphorylated (p)-mTOR, LC3 I/II and actin were used in subsequent experiments. Appropriate HRP-conjugated secondary antibodies were used for western blotting and fluorescent secondary antibodies were used for immunofluorescence staining.

Data acquisition and preprocessing. Publicly available OA-related datasets were retrieved from the Gene Expression Omnibus database (https://www.ncbi.nlm.nih.gov/geo/), including GSE114007 (38), GSE175961 (https://www.ncbi.nlm.nih.gov/geo/query/acc.cgi?acc=GSE175 961) and GSE51588 (39). GSE114007 was used to analyze OA-associated transcriptomic alterations and the HMGA2 expression patterns. GSE175961 was used for candidate miRNA prioritization and GSE51588 was used for co-expression analysis involving MIR155HG and HMGA2. Expression matrices and corresponding platform annotation files were downloaded and processed in R software (version 4.2.3; Posit Software, PBC). Probes were mapped to official gene symbols according to the platform annotation files. Probes without valid gene annotation were removed and when multiple probes corresponded to the same gene, the median expression value was used. Data normalization and preprocessing were performed using appropriate R packages, including 'limma' and 'sva', when required.

Differential expression analysis and HMGA2 expression evaluation. Differential expression analysis was performed using the 'limma' package in R (40). Genes with $\log_2$ fold change >1 and adjusted $P<0.05$ were considered to be differentially expressed. Hierarchical clustering heatmaps and box plots were generated using 'pheatmap' (41) and 'ggplot2' (42). HMGA2 expression level was compared between normal and OA cartilage samples. In addition, HMGA2 expression was compared across different clinical grades of cartilage degeneration, classified according to the Outerbridge grading system: Normal (grade 0, intact cartilage surface without lesions), grade 1 (cartilage softening and swelling with an intact surface) and grade 4 (full-thickness cartilage loss with exposed subchondral bone). Comparisons between two groups were performed using an unpaired two-tailed t-test and comparisons among multiple groups were performed using one-way ANOVA, followed by Tukey's post-hoc test.

Identification of HMGA2-related genes and pathway enrichment analysis. To explore the functional landscape associated with HMGA2 in OA, Pearson correlation analysis

Table II. Sequences of hsa-miR-212-3p mimics and inhibitors.

Name	Sequences
hsa-miR-212-3p mimic	5'-UAACAGUCUCCAGUCACGGCC-3', 3'-GGCCGUGACUGGAGACUGUUA-5'
Mimic NC	5'-UCACAACCUCCUAGAAAGAGUAGA-3', 3'-UCUACUCUUUCUAGGAGGUUGUGA-5'
hsa-miR-212-3p inhibitor	5'-GGCCGUGACUGGAGACUGUUA-3'
Inhibitor NC	5'-UCUACUCUUUCUAGGAGGUUGUGA-3'

miR, microRNA; NC, negative control.

was performed between HMGA2 and all transcriptome genes in the GSE114007 dataset. Genes significantly correlated with HMGA2 expression were defined as HMGA2-related genes using the criteria r>0.4 and P<0.05. Kyoto Encyclopedia of Genes And Genomes (KEGG) pathway (https://www.genome.jp/kegg/) enrichment analysis was performed using the 'clusterProfiler' R package (43).

Upstream competing endogenous RNA (ceRNA) regulatory axis of HMGA2 screening. To identify potential upstream non-coding RNA regulators of HMGA2, miRNAs predicted to target HMGA2 were independently retrieved from the TargetScan (https://www.targetscan.org/) and DIANA-microT databases (https://dianalab.e-ce.uth.gr/) and candidates shared by both databases were retained. Candidate miRNAs with valid expression measurements in the GSE175961 dataset were subsequently evaluated using SVM. SVM analysis was performed in R (version 4.3.1; Posit Software, PBC) using the svm() function in the 'e1071' R package (44). Each sample was treated as an independent observation, candidate miRNA expression levels were used as input features and disease status was specified as a binary outcome. OA cartilage samples in GSE175961 were designated as the positive class, whereas healthy control cartilage samples were designated as the negative class. Before model fitting, all miRNA expression features were centered and scaled. A linear-kernel SVM was constructed with the cost parameter set to 1. No additional class weights were applied because the positive and negative classes were balanced.

The relative importance of each candidate miRNA was assessed using the absolute value of its feature weight in the linear SVM decision function. A larger absolute weight indicated a greater contribution to the decision boundary separating OA from healthy control samples and candidate miRNAs were prioritized accordingly. HMGA2 was subsequently used as the anchor gene and Pearson correlation analysis was performed in the GSE51588 dataset to identify lncRNAs whose expression was associated with HMGA2 expression. The correlation results were integrated with miRNA-target prediction evidence to construct candidate lncRNA-miRNA-HMGA2 ceRNA regulatory axes for subsequent experimental validation.

ASO-MIR155HG,miR-212-3pmimicandmiR-212-3pinhibitor construction. ASO-MIR155HG sequences were designed following the human MIR155HG sequence obtained from GenBank (https://ngdc.cncb.ac.cn/). A number of candidate ASO sequences were synthesized. The ASO sequence with the highest interference efficiency was selected for subsequent functional assays. The hsa-miR-212-3p mimic, miR-212-3p inhibitor, mimic negative control and inhibitor negative control were synthesized according to the mature hsa-miR-212-3p sequences. The miR-212-3p mimic was used for dual-luciferase reporter assays, whereas the miR-212-3p inhibitor was used in rescue experiments to evaluate whether miR-212-3p mediated the effects of MIR155HG knockdown. The sequences of ASO-MIR155HG and ASO-NC are presented in Table I. The sequences of the hsa-miR-212-3p mimic, inhibitor, and their negative controls are listed in Table II. The ASO sequences listed in Table I are the synthesized antisense strands written in the 5'-3' direction. For sequence verification against MIR155HG RefSeq NR_001458.3, chemical-modification notation was removed, U was converted to T and each ASO sequence was reverse-complemented. All three ASOs exhibited complete sequence identity with their intended MIR155HG target sites. The mature hsa-miR-212-3p sequence is: 5'-UAACAGUCUCCAGUCACGGCC-3' (miRBase accession: MIMAT0000269; https://www.mirbase.org/). The sense strand of the miR-212-3p mimic was identical to the mature miRNA sequence, whereas the mimic antisense strand and the miR-212-3p inhibitor were designed as the complementary sequence, 5'-GGCCGUGACUGGAGACUGUUA-3'.

Flow cytometry analysis of apoptosis. Cell apoptosis was evaluated using an Annexin V-FITC/PI Apoptosis Detection Kit [cat. no. AP101-100; MultiSciences (Lianke) Biotech Co., Ltd.]. Briefly, the cells were harvested after treatment, washed twice with PBS and resuspended in binding buffer. Cells were then stained with Annexin V-FITC and propidium iodide for 10 min at room temperature in the dark. Apoptotic cells were detected using a NovoCyte 2060R flow cytometer [Acea Biosciences (Hangzhou) Co., Ltd.] and the apoptosis rates were quantified.

Flow cytometry analysis of ROS. Intracellular ROS levels were detected using DCFH-DA staining. After treatment, the cells were incubated with 10 μM DCFH-DA at 37˚C for 20 min in the dark. The cells were then washed thrice with serum-free medium and resuspended in PBS. Fluorescence intensity was measured using a NovoCyte 2060R flow cytometer [Acea Biosciences (Hangzhou) Co., Ltd.] and data were acquired and analyzed with FlowJo software (version 10.8.1; BD Biosciences). The geometric mean fluorescence intensity (gMFI) was used to quantify intracellular ROS accumulation.

Assessment of mitochondrial membrane potential. Mitochondrial membrane potential was assessed using a JC-1 staining kit (cat. no. BB-4105; BestBio Science Co., Ltd.). Briefly, the treated cells were harvested and incubated with JC-1 working solution at 37˚C for 20 min in the dark. After washing with JC-1 staining buffer, the cells were analyzed using a NovoCyte 2060R flow cytometer [Acea Biosciences (Hangzhou) Co., Ltd.]. Cellular debris was excluded based on forward and side scatter and the main cell population was selected for subsequent analysis. JC-1 fluorescence was analyzed using FITC and PE channels. Cells with relatively high mitochondrial membrane potential predominantly exhibited red fluorescence from JC-1 aggregates, whereas cells with decreased mitochondrial membrane potential revealed increased green fluorescence from JC-1 monomers. The green/red fluorescence ratio was used to quantify mitochondrial membrane potential changes, with an increased green/red ratio indicating mitochondrial membrane potential loss.

Transmission electron microscopy. After treatment, the cells were collected and fixed with 2.5% glutaraldehyde for 2 h at 4˚C, followed by post-fixation with 1% osmium tetroxide for 1 h at 4˚C. The samples were dehydrated using graded ethanol, embedded in epoxy resin and sectioned into ultrathin slices 70-nm thick. The sections were stained with uranyl acetate for 15 min at room temperature in the dark and subsequently with lead citrate for 10 min at room temperature, and examined using transmission electron microscopy to evaluate mitochondrial ultrastructural changes and identify autophagosome-like structures.

Immunofluorescence staining. Chondrocytes were fixed with 4% paraformaldehyde for 30 min at room temperature and permeabilized with 0.5% Triton X-100 for 20 min. After blocking with 5% BSA (cat. no. A8020; Beijing Solarbio Science & Technology Co., Ltd.) at 37˚C for 30 min, the cells were incubated overnight at 4˚C with primary antibodies against MMP13 (rabbit anti-MMP13; cat. no. AF5355; dilution 1:200; Affinity Biosciences, Ltd.) and COL2A1 (rabbit anti-COL2A1; cat. no. AF0135; dilution 1:200; Affinity Biosciences, Ltd.). The cells were then incubated with Cy3-conjugated goat anti-rabbit IgG (H+L) secondary antibody (cat. no. AS007; dilution 1:200; ABclonal Technology Co., Ltd.) for 1 h at 37˚C in the dark. The nuclei were counterstained with DAPI staining solution (cat. no. KGA1808-50; KeyGEN BioTECH Co., Ltd.) for 3 min at room temperature in the dark. Images were captured using a fluorescence microscope and the fluorescence intensity was quantified to evaluate changes in the extracellular matrix degradation-related markers.

RT-qPCR. Total RNA was extracted from the chondrocytes using TRIzon Reagent (cat. no. CW0580S; CWBIO/CoWin Biosciences), following the manufacturer's instructions. RNA concentration and purity were assessed using a NanoPhotometer spectrophotometer. cDNA was synthesized using a reverse transcription kit (cat. no. R223-01; Vazyme Biotech Co., Ltd.) and qPCR reagents (cat. no. CW3360M; CWBIO/CoWin Biosciences) was performed using a real-time PCR system. The reaction steps are as follows: Pre denature at 95˚C for 10 min; denaturation at 95˚C for 10 sec; annealing at 58˚C for 30 sec; extension at 72˚C for 30 sec; for 40 cycles. The RT-qPCR assay was used to detect MIR155HG and HMGA2 expression levels in the corresponding experiments. β-actin was used as the internal reference for mRNA and lncRNA detection. Relative expression levels were calculated using the $2^{-\Delta\Delta Cq}$ method (45). RT-qPCR was also used to evaluate the transfection efficiency of the miR-212-3p inhibitor by comparing miR-212-3p expression between cells transfected with the miR-212-3p inhibitor and those transfected with inhibitor NC. All primer sequences are listed in Table III.

Table III. Primer sequences.

Primer name	Primer sequence (5'-3')
β-actin F	TGGCACCCAGCACAATGAA
β-actin R	CTAAGTCATAGTCCGCCTAGA AGCA
HMGA2 F	AGACCTAGGAAATGGCCACAACA
HMGA2 R	ACTGCTGCTGAGGTAGAAATCG
LncMIR155HG F	GACCTTACCTGTCACCTTGGC
LncMIR 155HG R	AAAACCCCTATCACGATTAGCA

HMGA2, high mobility group AT-hook 2; F, forward; R, reverse; lnc, long non-coding RNA; MIR, microRNA.

Western blotting. Chondrocytes were lysed with RIPA lysis buffer (cat. no. C1053; Beijing Pulilai Gene Technology Co., Ltd.) to extract total protein. Cell lysates were centrifuged at ~13,500 x g) for 10 min at 4˚C and the supernatants were collected. Protein concentrations were determined using a BCA protein assay kit (cat. no. E-BC-K318-M; Elabscience Bionovation Inc.). Equal amounts of protein (20 μg per lane) were mixed with loading buffer, denatured and separated by 5/10% SDS-PAGE gel electrophoresis. The proteins were then transferred onto PVDF membranes (MilliporeSigma) at a constant current of 300 mA for 1 h. After blocking with 5% skimmed milk in TBST at room temperature for 1 h, the membranes were incubated overnight at 4˚C with primary antibodies against mTOR, p-mTOR, LC3 I/II and actin. After washing with TBST [20 mM Tris-HCl, 150 mM NaCl, 0.1% Tween-20 (pH 7.6)], the membranes were incubated with the corresponding HRP-conjugated secondary antibodies at room temperature for 2 h. Protein bands were visualized using an ECL substrate (cat. no. RJ239676; Thermo Fisher Scientific, Inc.) and images were acquired using a Tanon-5200 chemiluminescence imaging system (Tanon Science and Technology Co., Ltd.). The relative levels of p-mTOR/mTOR and LC3 II were quantified using grayscale analysis. All antibody information and dilutions are listed in Table IV.

Dual-luciferase reporter assay. The putative binding sites between miR-212-3p and MIR155HG or the HMGA2 3'UTR were predicted using the miRanda R package (46). Wild-type (WT) and mutant fragments of MIR155HG and the HMGA2 3'UTR containing the predicted miR-212-3p binding sites were synthesized and inserted into the pmirGLO luciferase reporter vector [synthesized by General Bio (Anhui) Co., Ltd.].

Table IV. Antibodies used for immunofluorescence staining and western blotting.

Antibody	Cat. no.	Supplier	Application	Dilution
Mouse Anti-β-actin	HC201	TransGen Biotech Co., Ltd.	Western blotting	1:2,000
Rabbit Anti p-mTOR	BS-3495R	BIOSS	Western blotting	1:1,000
Mouse Anti mTOR	66888-1-Ig	Proteintech Group, Inc.	Western blotting	1:10,000
HRP-conjugated Goat Anti-Mouse IgG (H+L)	GB23301	Wuhan Servicebio Technology Co., Ltd.	Western blotting	1:2,000
HRP-conjugated Goat Anti-Rabbit IgG (H+L)	GB23303	Wuhan Servicebio Technology Co., Ltd.	Western blotting	1:2,000
Rabbit Anti-MMP13	AF5355	Affinity Biosciences	Immunofluorescence	1:200
Rabbit Anti-COL2A1	AF0135	Affinity Biosciences	Immunofluorescence	1:200
Cy3-conjugated Goat Anti-Rabbit IgG	AS007	ABclonal Biotech Co., Ltd.	Immunofluorescence	1:200

COL2A1, type II collagen α 1 chain.

For the luciferase assay, 293T cells were seeded into plates and co-transfected with WT or mutant reporter plasmids together with miR-212-3p mimic or mimic NC [synthesized by General Bio (Anhui) Co., Ltd.] using Lipofectamine® 3000 (Thermo Fisher Scientific, Inc.) following the manufacturer's protocol. The sequence information of the miR-212-3p mimic and mimic NC is presented in Table II. After 48 h of transfection, the cells were collected and lysed in RIPA lysis buffer (cat. no. C1053; Beijing Pulilai Gene Technology Co., Ltd.) at 4˚C for 20 min. A total of 70 µl cell lysate from each group was transferred into a 96-well plate. At 48 h post-transfection, firefly luciferase activity was first measured after adding 100 µl luciferase assay reagent from the Dual Luciferase Reporter Gene Assay Kit (cat. no. RG027; Beyotime Biotechnology). *Renilla* luciferase activity was measured after adding 100 µl *Renilla* luciferase detection reagent. Relative luciferase activity was calculated by normalizing the firefly luciferase activity to *Renilla* luciferase activity.

Statistical analysis. Bioinformatics analyses were performed using R software (version 4.3.1; Posit Software, PBC) and associated packages, including 'limma', 'sva', 'clusterProfiler', 'pheatmap' and 'ggplot2'. The experimental data were analyzed using GraphPad Prism software (version 9.0; Dotmatics). All *in vitro* experiments were independently repeated thrice and the data are presented as the mean ± SD. For comparisons between the two groups, an unpaired two-tailed Student's t-test was used. For comparisons among multiple groups, one-way ANOVA followed by Tukey's post-hoc test was performed. Pearson correlation analysis was used to evaluate the relationship between gene expression levels in public datasets. P<0.05 was considered to indicate a statistically significant difference.

Results

HMGA2 is identified as an OA-associated candidate gene. To identify the core genes driving OA progression, the present study conducted a differential transcriptome analysis of the GSE114007 dataset. Hierarchical clustering analysis revealed that the screened differentially expressed genes effectively distinguished OA samples from normal controls, with HMGA2 exhibiting a distinct upregulation signature in OA tissues (Fig. 1A; Table SI). Quantitative analysis verified that HMGA2 expression was significantly elevated in OA cartilage compared with the normal group (P<0.0001; Fig. 1B). Furthermore, trend analysis across different clinical grades revealed a significant stepwise increase in HMGA2 levels as the disease progressed, with peak expression observed in Grade 4 OA samples (P<0.0001; Fig. 1C).

HMGA2 correlates with mTOR-related signaling and autophagy pathway dysregulation. Functional enrichment analysis was conducted to assess the biological processes associated with HMGA2-related genes. KEGG enrichment results revealed that these genes were enriched in numerous OA- and autophagy-associated pathways, including the 'mTOR signaling pathway' [normalized enrichment score (NES)=1.75; P<0.01], 'phosphatidylinositol signaling system' (NES=2.08; P<0.001), 'osteoclast differentiation' (NES=2.01; P<0.001), 'NF-κB signaling pathway' (NES=1.73; P<0.01), 'cellular senescence' (NES=1.68; P<0.01) and 'autophagy' (NES=1.59; P=0.016; Fig. 1D; Table SII). The synergistic correlation matrix further revealed that HMGA2 expression was strongly positively correlated with the mTOR upstream activator Akt3 (r=0.79), autophagy substrate sequestosome-1/p62 (r=0.78) and matrix-degrading enzyme MMP13 (r=0.56). Conversely, HMGA2 revealed a distinct negative correlation with the cartilage protective factor COL2A1 (r=-0.67) and the mTOR downstream effector ribosomal protein S6 kinase β-2 (r=-0.57; Fig. 1E; Table SIII). Collectively, these bioinformatic data suggest that HMGA2 is closely associated with mTOR-related signaling, autophagy dysregulation and extracellular matrix imbalance in OA chondrocytes.

The MIR155HG/miR-212-3p/HMGA2 axis is identified through machine learning. To elucidate the upstream regulatory network of HMGA2, the present study integrated bioinformatics prediction with machine learning models. Intersection analysis of the TargetScan and DIANA-microT databases identified eight conserved candidate miRNAs

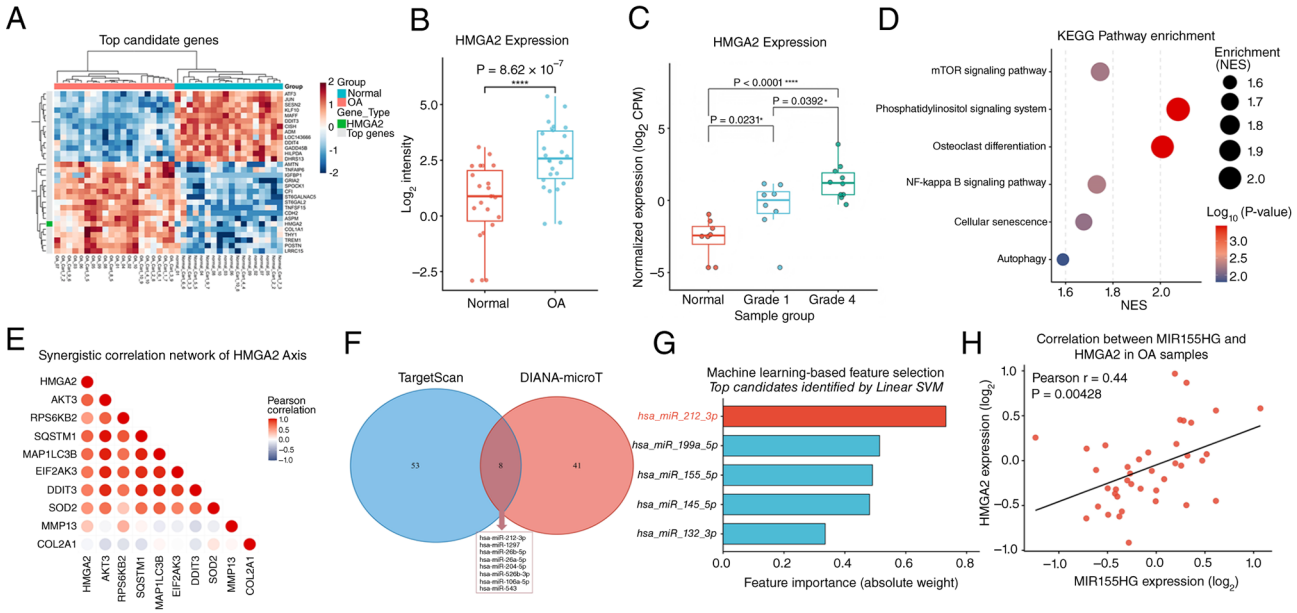


Figure 1. Identification of HMGA2 as a key candidate gene and MIR155HG/miR-212-3p/HMGA2 ceRNA network construction in OA. (A) Hierarchical clustering heatmap of the top candidate genes between normal and OA cartilage samples in the GSE114007 dataset. (B) Comparison of HMGA2 expression levels between the normal and OA groups. (C) Stepwise increase in HMGA2 expression across clinical grades, including Normal, Grade 1 and Grade 4. (D) Kyoto Encyclopedia of Genes and Genomes pathway enrichment analysis exhibiting significant involvement of the mTOR signaling pathway and autophagy. (E) Pearson correlation matrix revealing the association between HMGA2 and markers of the mTOR pathway, autophagy and matrix metabolism. (F) Venn diagram identifying eight conserved miRNAs targeting HMGA2 predicted by the TargetScan and DIANA-microT databases. (G) Ranking of candidate miRNAs using a linear SVM model, with hsa-miR-212-3p exhibiting the highest feature importance. (H) Pearson correlation scatter plot depicting the positive association between lncRNA MIR155HG and HMGA2 expression in OA samples. *P<0.05 and ****P<0.0001. HMGA2, high mobility group AT-hook 2; OA, osteoarthritis; ceRNA, competitive endogenous RNA; miR/MIR, microRNA; SVM, support vector machine; NES, normalized enrichment score; CPM, counts per million; SOD2, superoxide dismutase 2; COL2A1, type II collagen α 1 chain; SQSTM1, sequestosome-1; RPS6KB2, ribosomal protein S6 kinase B2; MAP1LC3B, microtubule-associated protein 1 light chain 3 β.

that potentially target HMGA2 (Fig. 1F). Using a linear SVM model to rank these candidates based on their feature importance in the GSE175961 dataset, hsa-miR-212-3p was identified as the top-ranking node with the highest absolute weight (0.73), indicating its pivotal role in OA pathological classification (Fig. 1G; Table SIV). Subsequently, co-expression analysis using the GSE51588 dataset revealed that lncRNA MIR155HG expression was moderately positively correlated with HMGA2 expression (r=0.44; P=0.00428; Fig. 1H). Based on these findings, the present study proposed the MIR155HG/miR-212-3p/HMGA2 axis as a candidate regulatory network potentially associated with mTOR-related and autophagy-related signaling in OA chondrocytes.

Interference with lncRNA MIR155HG inhibits IL-1β-induced apoptosis and mitochondrial damage. An IL-1β-induced inflammation model was constructed and qPCR was used to detect lncMIR155HG levels in cells (Fig. 2A). Compared with the Control group, the lncMIR155HG level in the Model group was significantly increased (P<0.001). lncMIR155HG ASOs were synthesized to interfere with lncMIR155HG and the ASO with the most notable interference effect was selected through qPCR detection (Fig. 2B). Compared with ASO-NC, transfection with lncMIR155HG ASOs significantly reduced the expression level of lncMIR155HG (P<0.0001), among which ASO-417 exhibited the most significant interference effect (P<0.0001). Therefore, ASO-417 was selected for the subsequent experiments.

The immortalized chondrocytes were transfected with ASO-417 and inflammation was induced with IL-1β. The cells were collected and apoptosis, intracellular ROS levels and mitochondrial membrane potential were assessed by flow cytometry. Compared with the Control group, the Model group exhibited a significant increase in apoptosis rate and ROS gMFI, together with a significant increase in JC-1 green/red fluorescence ratio (P<0.0001). Compared with the Model + ASO-NC group, the Model + ASO-lncMIR155HG group depicted a significant decrease in apoptosis rate, ROS gMFI and the JC-1 green/red fluorescence ratio (P<0.0001). These results indicated that IL-1β induced chondrocyte apoptosis, ROS accumulation and mitochondrial membrane potential loss, whereas interference with lncMIR155HG attenuated these changes (Fig. 2C). In the Control group, the mitochondria exhibited intact outer and inner membranes, clearly defined cristae and normal matrix electron density (blue arrows). Morphologically normal rough endoplasmic reticulum (yellow arrows) and Golgi apparatus (green arrows) were also observed. In Model and Model + ASO-NC groups, mitochondria exhibited shrinkage and disruption or loss of cristae and autophagosome-like structures were observed in the cytoplasm (orange arrows). In the Model + ASO-lncMIR155HG group, mitochondrial ultrastructural damage was attenuated, with relatively preserved outer membranes and cristae. Autophagosome-like structures were also observed. These findings indicated that MIR155HG knockdown attenuated IL-1β-induced mitochondrial ultrastructural damage (Fig. 2D). The mean ROS gMFI values were 894,372, 2,073,438, 2,131,325 and 1,030,084 in the Control, Model, Model + ASO-NC and Model + ASO-lncMIR155HG groups, respectively.

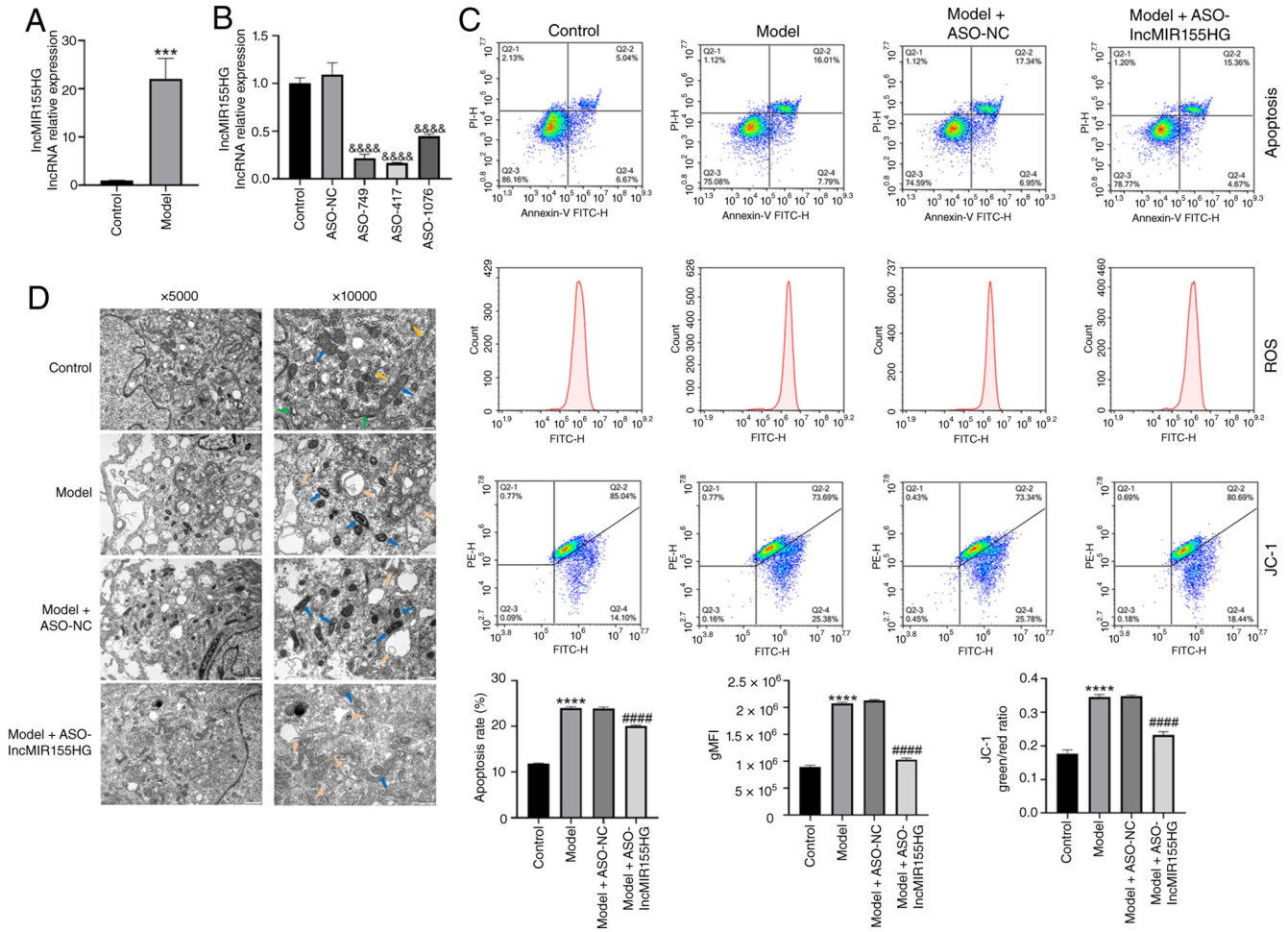


Figure 2. Effects of lncMIR155HG interference on IL-1β-induced apoptosis and mitochondrial damage. (A) qPCR detection of lncMIR155HG expression in the cell inflammatory model (n=3). (B) Interference efficiency of lncMIR155HG antisense oligonucleotides validated by qPCR (n=3). (C) Flow cytometry analysis of apoptosis, intracellular ROS levels quantified using gMFI and mitochondrial membrane potential evaluated using the JC-1 green/red fluorescence ratio (n=3). (D) Representative transmission electron microscopy images exhibiting mitochondrial ultrastructural changes and autophagosome-like structures. Blue arrows indicate mitochondrial structures, yellow arrows indicate the rough endoplasmic reticulum, green arrows indicate the Golgi apparatus and orange arrows indicate autophagosome-like structures. Images are presented at x5,000 and x10,000 magnification (scale bars, 1 μm and 500 nm; n=3). ***P<0.001 and ****P<0.0001 compared with the Control group. $^{\#\#\#\#}$P<0.0001 compared with the Model + ASO-NC group. $^{\&\&\&\&}$P<0.0001 compared with the ASO-NC group. qPCR, quantitative PCR; lnc, long non-coding RNA; MIR, microRNA; ROS, reactive oxygen species; NC, negative control; ASO, antisense oligonucleotide; gMFI, geometric mean fluorescence intensity.

Interference with lncRNA MIR155HG inhibits IL-1β-induced cartilage matrix degradation. Immunofluorescence detection was used to detect MMP13 and COL2A1 expression in each group of cells (Fig. 3A and B). Compared with the Control group, MMP13 expression in the Model group was significantly increased (P<0.0001), whereas COL2A1 expression was significantly decreased (P<0.0001). Compared with the Model+ASO-NC group, the Model+ASO-lncMIR155HG group revealed a significant decrease in MMP13 expression (P<0.0001) and a significant increase in COL2A1 expression (P<0.0001). The results suggested that IL-1β could induce high expression of MMP13 in chondrocytes, which can degrade COL2A1 in the cartilage matrix, leading to OA, while interference with lncMIR155HG inhibited IL-1β-induced cartilage matrix degradation.

miR-212-3p interacts with lncRNA MIR155HG and HMGA2. lncMIR155HG, HMGA2 WT and mutant dual luciferase vectors were constructed, miR-212-3p mimic and mimic NC were synthesized and they were transfected into cells to verify whether miR-212-3p targets lncMIR155HG and HMGA2. As shown in Fig. 4A and B, compared with the WT lncMIR155HG + mimic NC group, the fluorescence intensity of the WT lncMIR155HG + miR-212-3p mimic group was significantly reduced (P<0.01). There was non-significant difference in fluorescence intensity between MUT lncMIR155HG + mimic NC and MUT lncMIR155HG + miR-212-3p mimic groups observed (P>0.05). These results indicated an interaction between lncMIR155HG and miR-212-3p. Compared with the WT-HMGA2 + mimic NC group, the fluorescence intensity of the WT-HMGA2 + miR-212-3p mimic group was significantly reduced (P<0.01). There was non-significant difference in fluorescence intensity between MUT-HMGA2 + mimic NC and MUT-HMGA2 + miR-212-3p mimic groups (P>0.05). These results indicated an interaction between miR-212-3p and HMGA2.

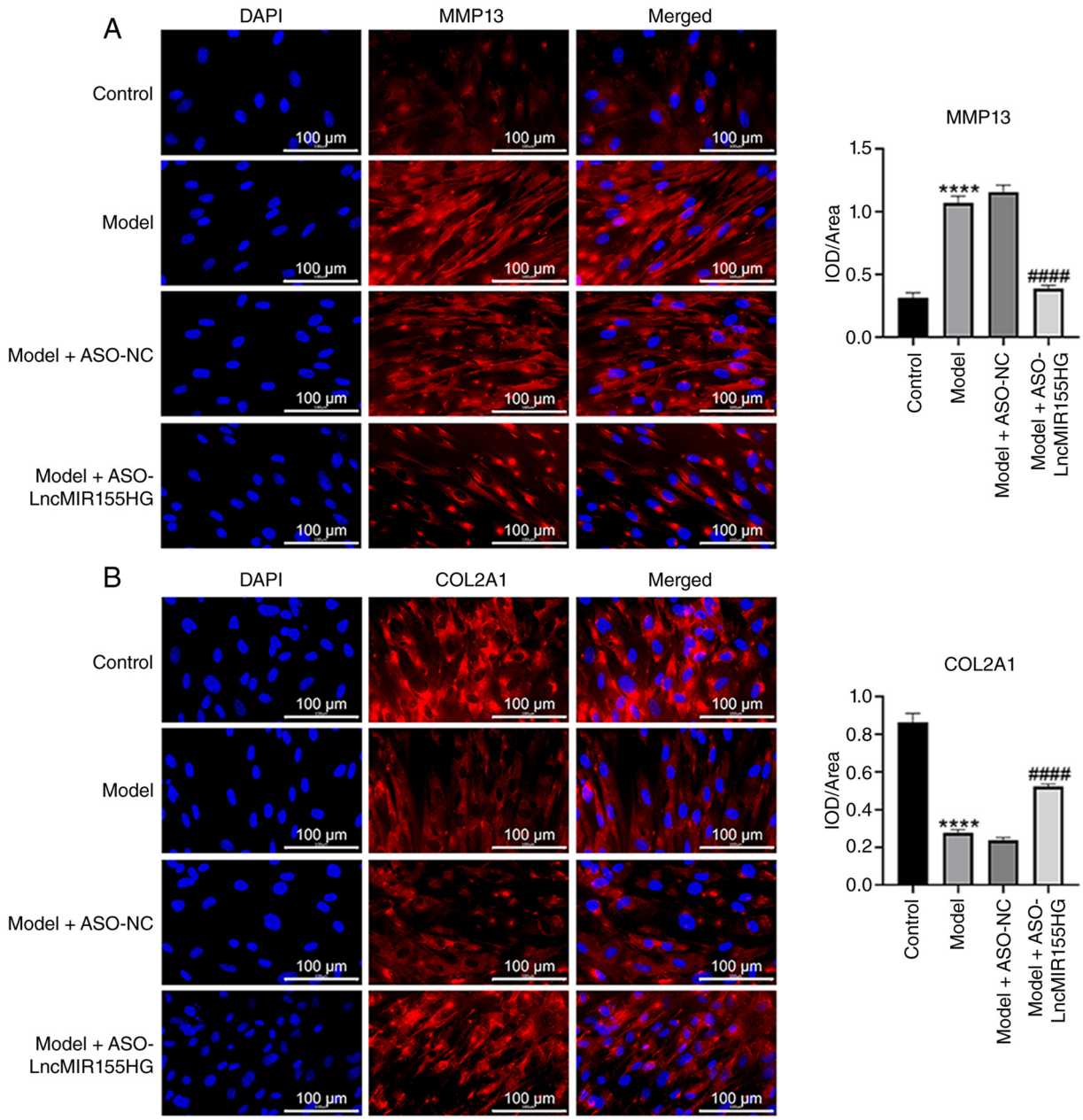


Figure 3. Effects of lncMIR155HG interference on cartilage matrix degradation. (A) Immunofluorescence detection of MMP13 expression in cells (scale bar, 100 μm; n=3). (B) Immunofluorescence detection of COL2A1 expression in cells (scale bar, 100 μm; n=3). The immunofluorescence intensity of MMP13 and COL2A1 was quantified as the integrated optical density per unit area (IOD/Area, i.e., the IOD of the positive staining normalized to the measured field area, reflecting the mean staining intensity per unit area) using ImageJ software (National Institutes of Health). ****P<0.0001 compared with the Control group and $^{####}$P<0.0001 compared with the Model + ASO-NC group. Lnc, long non-coding RNA; ASO, antisense oligonucleotide; COL2A1, type II collagen α 1 chain; NC, negative control; MIR, microRNA; IOD, integrated optical density.

lncRNA MIR155HG regulates apoptosis and mitochondrial damage through miR-212-3p. To investigate whether lncMIR155HG affects OA model cells through miR-212-3p, a miR-212-3p inhibitor was transfected into OA model cells. The inhibitory efficiency of the miR-212-3p inhibitor was first verified by RT-qPCR. Compared with the inhibitor NC group, miR-212-3p expression was significantly reduced after transfection with the miR-212-3p inhibitor (n=3; P<0.001; Fig. S1), demonstrating effective inhibition of miR-212-3p. Apoptosis, intracellular ROS levels and mitochondrial membrane potential were subsequently assessed by flow cytometry. As shown in Fig. 5, compared with the Model + inhibitor NC + ASO-NC group, MIR155HG knockdown significantly decreased the apoptosis rate (P<0.0001), ROS gMFI (P<0.01) and the JC-1 green/red fluorescence ratio (P<0.05). Conversely, inhibition of miR-212-3p exhibited opposite effects (P<0.0001). Compared with the Model + inhibitor NC + ASO-lncMIR155HG group, combined MIR155HG knockdown and miR-212-3p inhibition significantly increased the apoptosis rate (P<0.0001) and JC-1 green/red fluorescence ratio (P<0.001). Compared with the Model + miR-212-3p inhibitor + ASO-NC group, combined MIR155HG knockdown and miR-212-3p inhibition significantly reduced the apoptosis rate (P<0.0001), ROS gMFI (P<0.0001) and JC-1 green/red fluorescence ratio (P<0.0001).

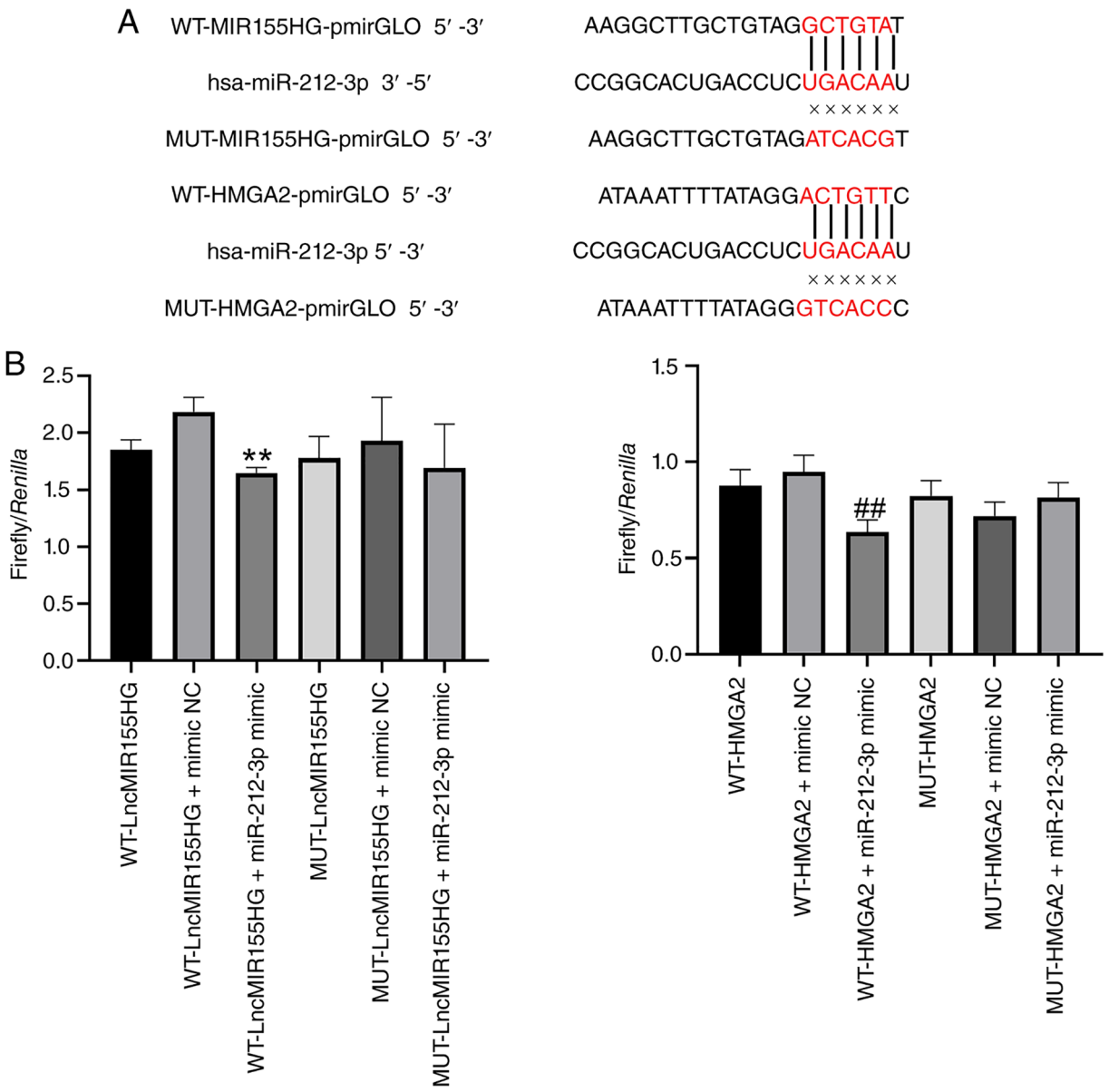


Figure 4. Interaction between miR-212-3p, lncMIR155HG and HMGA2 verified by dual-luciferase reporter assay. (A) Sequences of WT and MUT lncMIR155HG and HMGA2. (B) Results of the dual-luciferase reporter assay (n=3). **P<0.01 compared with the WT-MIR155HG + mimic NC group and $^{\#\#}$P<0.01 compared with the WT-HMGA2 + mimic NC group. miR/MIR, microRNA; lnc, long non-coding RNA; HMGA2, high mobility group AT-hook 2; WT, wild-type; MUT, mutant; NC, negative control.

These results indicated that lncMIR155HG regulates chondrocyte apoptosis and mitochondrial dysfunction through miR-212-3p in the OA-like cell model.

MIR155HG/miR-212-3p axis is associated with HMGA2 expression and mTOR-related autophagy signaling. The regulatory effect of miR-212-3p on HMGA2 and mTOR-related signaling was further examined in rescue experiments. RT-qPCR results revealed that HMGA2 mRNA expression was significantly decreased after MIR155HG knockdown in the Model + inhibitor NC + ASO-lncMIR155HG group compared with the Model + inhibitor NC + ASO-NC group (P<0.001). miR-212-3p inhibition further significantly increased HMGA2 expression in the Model + miR-212-3p inhibitor + ASO-NC group (P<0.01). In the combined treatment group, HMGA2 expression was significantly lower compared with the Model + miR-212-3p inhibitor + ASO-NC group (P<0.01); however, it was higher compared with the Model + inhibitor NC + ASO-lncMIR155HG group (P<0.0001; Fig. 6A).

Western blotting revealed similar changes in mTOR-related signaling. MIR155HG knockdown significantly reduced the p-mTOR/mTOR level (P<0.05) and significantly increased LC3 II protein expression (P<0.001). miR-212-3p inhibition significantly increased the p-mTOR/mTOR level (P<0.0001) and reduced LC3 II expression (P>0.05). Compared with the Model + inhibitor NC + ASO-lncMIR155HG group, combined treatment with the miR-212-3p inhibitor partly increased p-mTOR/mTOR (P<0.001) and decreased LC3 II expression (P<0.01). Compared with the Model + miR-212-3p inhibitor + ASO-NC group, ASO-lncMIR155HG partially reversed these changes (Fig. 6B-D).

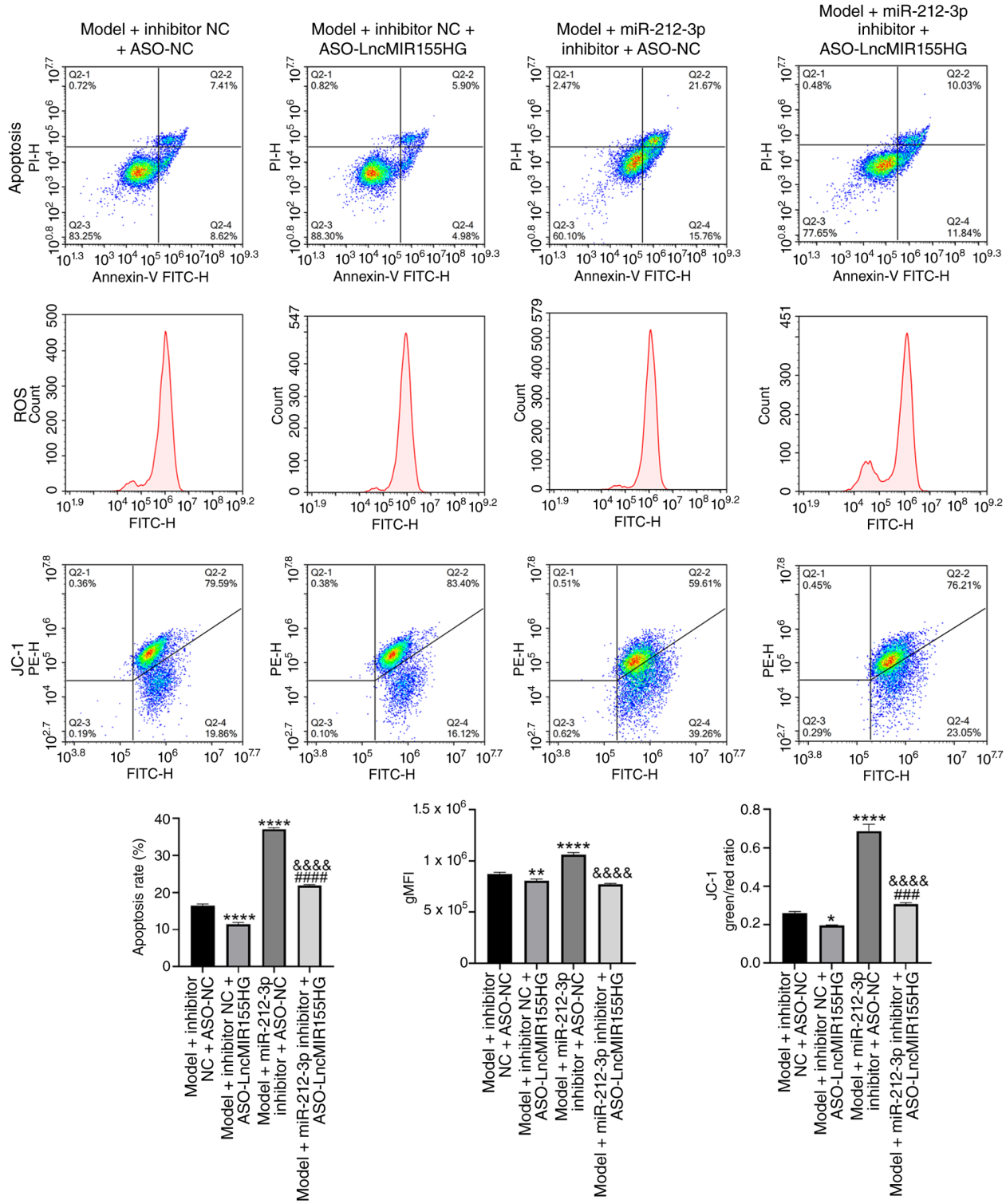


Figure 5. miR-212-3p inhibition partially reverses the effects of MIR155HG knockdown on IL-1β-induced chondrocyte injury. Flow cytometry analysis of apoptosis, intracellular ROS levels quantified using gMFI and mitochondrial membrane potential evaluated using the JC-1 green/red fluorescence ratio in chondrocytes subjected to MIR155HG knockdown and/or miR-212-3p inhibition (n=3). *P<0.05, **P<0.01 and ****P<0.0001 compared with the Model + inhibitor NC + ASO-NC group; $^{###}$P<0.001 and $^{####}$P<0.0001 compared with the Model + inhibitor NC + ASO-MIR155HG group; and $^{&&&&}$P<0.0001 compared with the Model + miR-212-3p inhibitor + ASO-NC group. miR/MIR, microRNA; ROS, reactive oxygen species; gMFI, geometric mean fluorescence intensity; NC, negative control; ASO, antisense oligonucleotide; lnc, long non-coding RNA.

Discussion

OA is the most common chronic degenerative joint disease (47). Cartilage is an important component of joints and chondrocytes are the only cells in cartilage that maintain cartilage integrity and ensure joint function by secreting the extracellular matrix (48). OA pathogenesis is complex and involves genetic, metabolic and biochemical factors (49). Mass chondrocyte death is key to OA development. Apoptosis is the main mode of chondrocyte death and autophagy can prevent

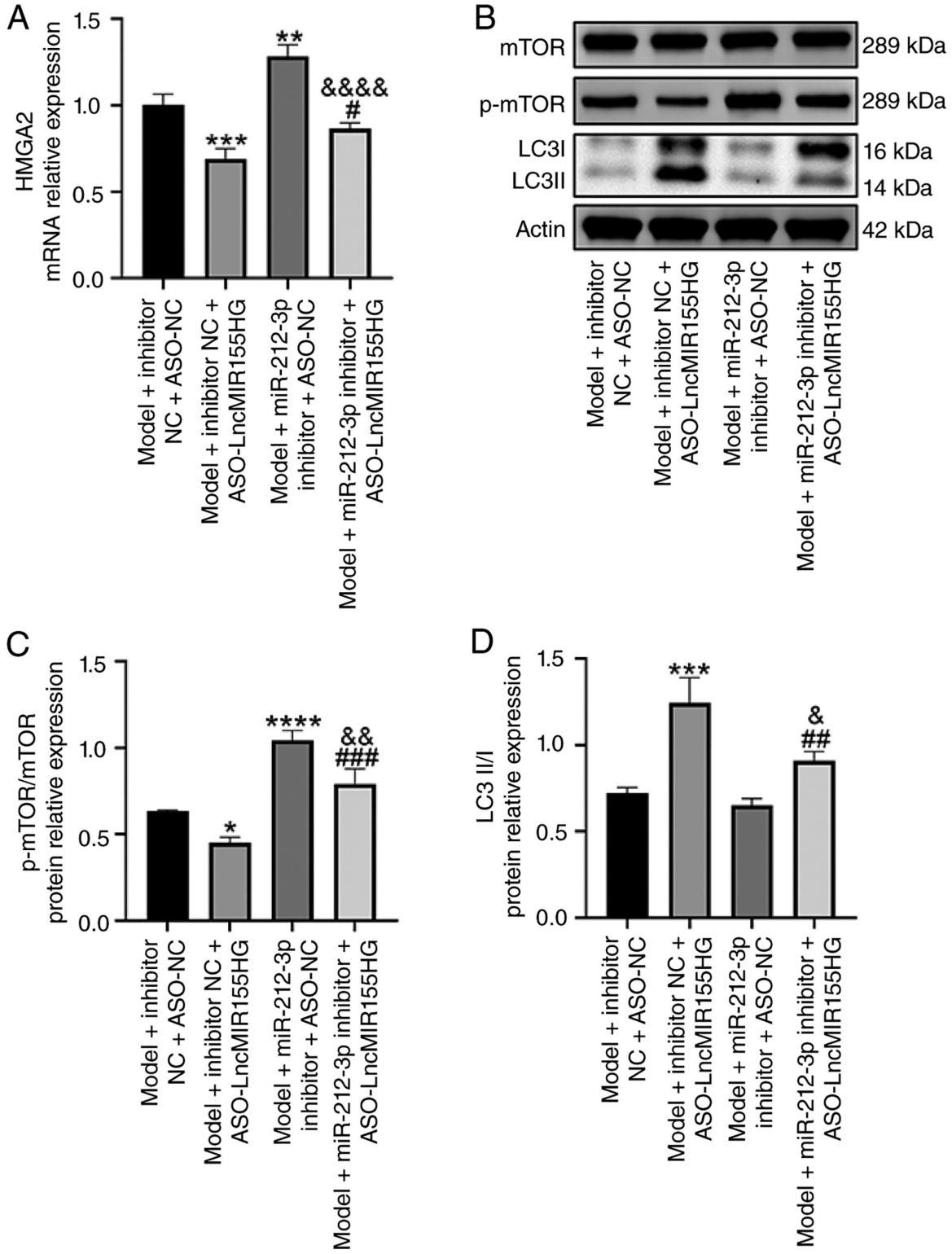


Figure 6. Effects of MIR155HG and miR-212-3p interference on HMGA2 expression and mTOR-related autophagy signaling in IL-1β-induced chondrocytes. (A) Reverse transcription-quantitative PCR analysis of HMGA2 mRNA expression in rescue experiments (n=3). (B) Representative western blotting of mTOR, p-mTOR, LC3 I, LC3 II and actin in each group. (C) Quantitative analysis of relative p-mTOR/mTOR protein expression (n=3). (D) Quantitative analysis of relative LC3 II protein expression (n=3). *P<0.05, **P<0.01, ***P<0.001 and ****P<0.0001 compared with the Model + inhibitor NC + ASO-NC group; $^{\#}$P<0.05, $^{\#\#}$P<0.01 and $^{\#\#\#}$P<0.001 compared with the Model + inhibitor NC + ASO-MIR155HG group and; $^{\&}$P<0.05, $^{\&\&}$P<0.01 and $^{\&\&\&\&}$P<0.0001 compared with the Model + miR-212-3p inhibitor + ASO-NC group. miR/MIR, microRNA; HMGA2, high mobility group AT-hook 2; NC, negative control; ASO, antisense oligonucleotide; p-, phosphorylated; lnc, long non-coding RNA.

apoptosis by clearing abnormal proteins and damaged organelles in cells (17). A number of studies have revealed that OA development is associated with apoptosis and autophagy, thus activating autophagy may be a notable strategy for treating OA. lncRNA can regulate gene expression at the transcriptional level, thereby affecting cell proliferation, apoptosis

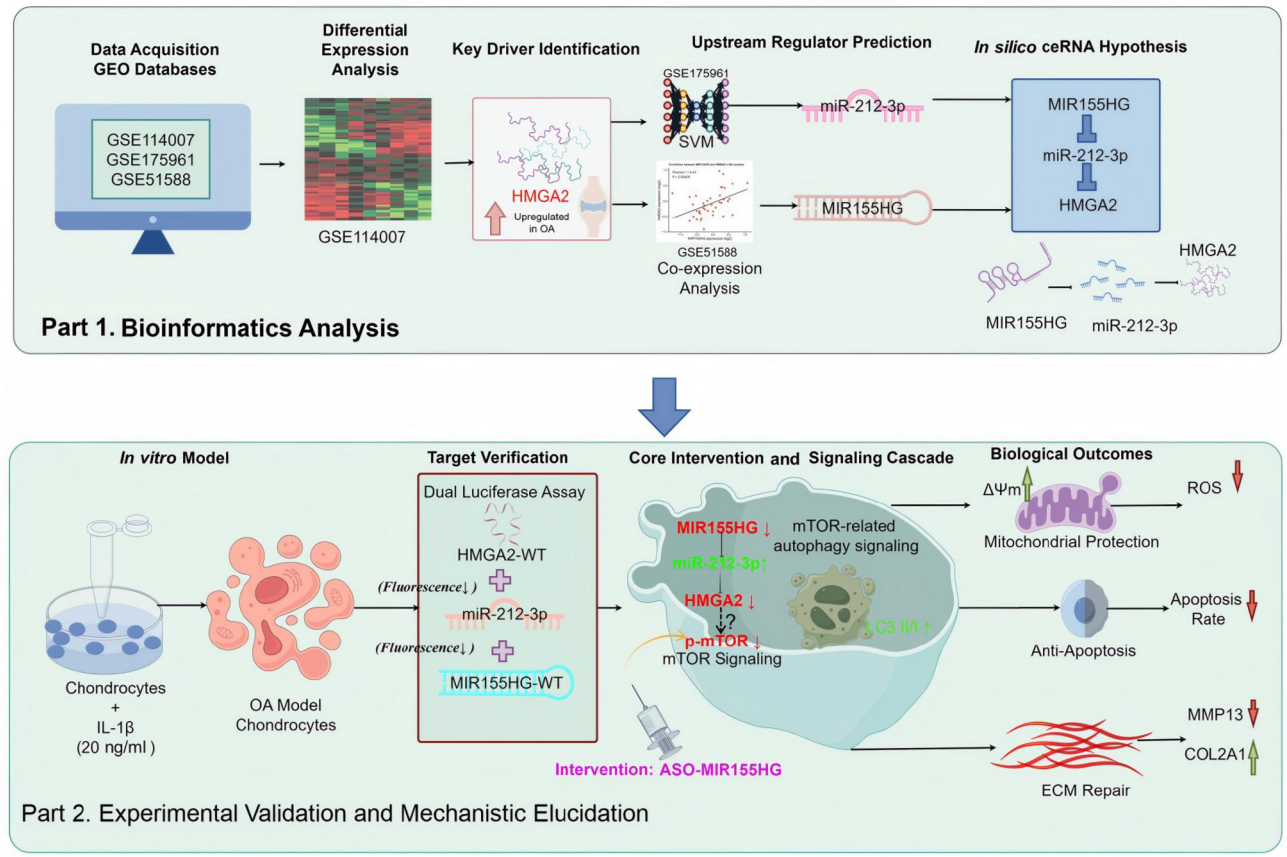


Figure 7. Proposed model of the MIR155HG/miR-212-3p/HMGA2 regulatory axis in OA-related chondrocyte injury. Integrated bioinformatics analysis identified HMGA2 as an OA-associated candidate gene and suggested the MIR155HG/miR-212-3p/HMGA2 axis as a potential ceRNA regulatory network. In IL-1β-induced chondrocytes, MIR155HG knockdown attenuated apoptosis, ROS accumulation, mitochondrial dysfunction and extracellular matrix degradation. Functional rescue experiments further suggested that these effects were at least partly mediated by miR-212-3p and associated with changes in HMGA2 expression and mTOR-related autophagy signaling. OA, osteoarthritis; lnc, long non-coding RNA; miR/MIR, microRNA; ASO, antisense oligonucleotide; HMGA2, high mobility group AT-hook 2; ROS, reactive oxygen species; ceRNA, competitive endogenous RNA; GEO, Gene Expression Omnibus; SVM, support vector machine; WT, wild-type; p-, phosphorylated; COL2A1, type II collagen α 1 chain.

and autophagy. It was observed that lncMIR155HG promoted the development of OA and lncMIR155HG could inhibit the activation of autophagy in mice with spinal cord injury (29), suggesting a potential association between MIR155HG and autophagy-related regulation, although whether a similar mechanism occurs in OA remains unclear. HMGA2, as a pro-inflammatory gene, is highly expressed in OA mice and autophagy is activated in HMGA2 knockout mice (36). Bioinformatics analysis also revealed that HMGA2 expression was upregulated in OA and positively correlated with disease grading. Prediction using the SVM algorithm revealed that MIR155HG and miR-212-3p may be upstream regulatory factors of HMGA2.

Therefore, the present study hypothesized that the MIR155HG/miR-212-3p/HMGA2 axis may be involved in apoptosis and autophagy-related signaling in OA. To examine this hypothesis, an OA-like cell injury model was established by treating human immortalized chondrocytes with IL-1β. MIR155HG knockdown was found to have attenuated chondrocyte apoptosis, ROS accumulation, mitochondrial dysfunction and extracellular matrix degradation. Rescue experiments further suggested that these effects were partly associated with miR-212-3p and HMGA2-associated signaling. miR-212-3p inhibition partially reversed the protective effects of MIR155HG knockdown. Furthermore, the present study observed that miR-212-3p has targeted binding sites with lncMIR155HG and HMGA2. These findings suggest that the MIR155HG/miR-212-3p/HMGA2 axis may be associated with mTOR-related autophagy signaling and may participate in IL-1β-induced chondrocyte apoptosis and matrix degradation (Fig. 7).

Oxidative stress is an important mechanism in OA pathogenesis and can lead to chondrocyte apoptosis. Mitochondrial dysfunction is a primary factor in activating oxidative stress. As well as serving organelles as an energy supply, mitochondria can produce signals that affect cellular function and metabolism (50). A previous study revealed that mitochondrial apoptosis is associated with chondrocyte apoptosis in OA (51). In addition, mitochondria are the main site for ROS production, which can promote the release of pro-inflammatory cytokines and metalloproteinase production. In OA development, a decrease in mitochondrial membrane potential leads to mitochondrial dysfunction, increased ROS generation and chondrocyte apoptosis (52). In the present study, IL-1β increased the apoptosis rate, ROS gMFI and the JC-1 green/red fluorescence ratio, indicating increased oxidative stress and mitochondrial membrane potential loss (53). MIR155HG knockdown attenuated these injury-related

changes. Mitochondrial structure was observed under transmission electron microscopy, showing that IL-1β treatment resulted in severe mitochondrial damage in chondrocytes, while interference with lncMIR155HG may attenuate mitochondrial damage. Degradation of the extracellular matrix in chondrocytes is a pathological change in OA development and COL2A1 is the main component of the extracellular matrix synthesized by chondrocytes (54). MMP13 is a member of the MMP family that can dissolve collagen. It has been reported that MMP13 is the main collagenase that degrades the extracellular matrix and is highly expressed in patients with OA (55). Consequently, a decrease in COL2A1 synthesis by chondrocytes and an increase in MMP13 expression are key events within, as well as pathogenic causes of, OA. The immunofluorescence results of the present study revealed that after IL-1β treatment, MMP13 expression was increased and COL2A1 expression was decreased. Interference with lncMIR155HG reduced MMP13 expression and increased COL2A1 expression, indicating that lncMIR155HG knockdown attenuated IL-1β-induced extracellular matrix degradation in chondrocytes.

Autophagy can prevent OA development by maintaining cellular homeostasis and preventing apoptosis activation (56). Autophagy initiation originates from phagosome formation with a bilayer membrane structure, which encapsulates organelles or proteins that need to be degraded to form autophagosomes. Autophagosomes then bind to lysosomes to form autolysosomes, thereby breaking down the substances within the autophagosomes. During this process, cytosolic LC3-I is conjugated to phosphatidylethanolamine to form LC3-II, which is recruited to autophagosomal membranes and is commonly used as an autophagosome-associated marker (57). However, LC3-II accumulation alone cannot distinguish increased autophagosome formation from impaired autophagosome degradation. Autophagy is regulated by numerous signaling pathways, among which mTOR is an important negative regulator. Previous studies have revealed that the inhibition of mTOR signaling can promote autophagy. For example, artemisinin activates autophagy by reducing the expression of tumor necrosis factor superfamily member 11 and inhibiting PI3K/Akt/mTOR signaling, thereby relieving OA (58); PG545 prevents the development of osteoarthritis by regulating PI3K/AKT/mTOR signaling, activating chondrocyte autophagy, reducing oxidative stress and chondrocyte apoptosis (59). In the present rescue experiments, MIR155HG knockdown reduced the relative p-mTOR/mTOR level and increased LC3 II protein expression, whereas miR-212-3p inhibition partially reversed these changes. These findings suggest that MIR155HG/miR-212-3p signaling is associated with mTOR-related autophagy signaling in IL-1β-induced chondrocytes. Furthermore, rescue experiments revealed that MIR155HG knockdown reduced HMGA2 mRNA expression, whereas miR-212-3p inhibition partially counteracted this effect. Wang and Li (60) revealed that lncMIR155HG could target miR-212-3p to regulate CD226 expression and inhibit lung adenocarcinoma cell proliferation, migration and apoptosis. An additional study revealed that miR-212-3p could target HMGA2 to inhibit its expression, thereby suppressing the proliferation, migration and apoptosis of osteosarcoma cells (61). The 'miRanda' database also predicts the existence of targeted binding sites between miR-212-3p, lncMIR155HG and HMGA2. The present dual-luciferase reporter assay demonstrated a direct interaction between miR-212-3p, MIR155HG and HMGA2, supporting the existence of an MIR155HG/miR-212-3p/HMGA2 regulatory axis.

The role of miR-212-3p may vary depending on the cellular and biological context. Previous studies have reported that osteoclast-derived exosomal miR-212-3p promotes chondrocyte dysfunction by targeting TGF-β1/Smad2 signaling, whereas miR-212-3p exerts anti-inflammatory effects by targeting HMGB1 (62,63). In the present study, miR-212-3p inhibition partially reversed the protective effects of MIR155HG knockdown in IL-1β-stimulated chondrocytes. These differences may be associated with the cellular origin of miR-212-3p, its downstream targets and the specific inflammatory microenvironment. Specifically, osteoclast-derived miR-212-3p is delivered to chondrocytes within exosomes and thus acts in a paracrine, vesicle-dependent manner, whereas the miR-212-3p manipulated in the present experiments functioned cell-autonomously within chondrocytes, where its free level is additionally buffered by lncRNA sponging (for example, by MIR155HG); the two pools are therefore subject to different regulation and can produce opposite outcomes. Moreover, miRNA target engagement is context-dependent: the repertoire of available target mRNAs varies with the transcriptional and pathological state of the cell, so miR-212-3p suppresses TGF-β1/Smad2 or HMGB1 in other models but predominantly regulates the MIR155HG/HMGA2 axis and mTOR-related autophagy signaling in IL-1β-stimulated chondrocytes, as shown here. Finally, the cytokine milieu itself shapes miR-212-3p function, as pro-inflammatory stimuli such as IL-1β alter both miR-212-3p expression and the abundance of its target transcripts, shifting the balance between its protective and detrimental effects. Taken together, the net effect of miR-212-3p in OA depends on its cellular source, the target network available in a given cell type and the inflammatory context, which reconciles the apparently conflicting reports in the literature.

To demonstrate whether lncMIR155HG affects apoptosis and autophagy by regulating miR-212-3p, an miR-212-3p inhibitor was transfected into chondrocytes. Flow cytometry revealed that interference with lncMIR155HG reduced the apoptosis rate, ROS level and proportion of cells with decreased mitochondrial membrane potential. However, these changes were reversed by interfering with lncMIR155HG and miR-212-3p through reverse complementary sequences, indicating that lncMIR155HG regulates apoptosis and mitochondrial damage through miR-212-3p. The qPCR results of the present study revealed that interference with lncMIR155HG decreased the expression level of HMGA2 mRNA, whereas interference with miR-212-3p increased the expression level of HMGA2 mRNA, indicating that lncMIR155HG regulates HMGA2 expression through miR-212-3p. Western blotting revealed that MIR155HG knockdown reduced the relative p-mTOR/mTOR level and increased LC3 II protein expression. Interfering with lncMIR155HG and miR-212-3p could therefore increase the relative expression of p-mTOR/mTOR and decrease the relative expression of LC3 II/I. These data suggest that the

MIR155HG/miR-212-3p/HMGA2 axis may be associated with mTOR-related autophagy signaling changes in OA-like chondrocytes.

Despite this, the present study only demonstrated an association between HMGA2 and the mTOR pathway, and the specific mechanism by which HMGA2 regulates mTOR signaling remains unclear. Evidence from gastric cancer cells clarifies both the relevance of this association and the direction of regulation: in that model, the lncRNA HIT000218960 upregulated HMGA2 protein expression, and HMGA2 knockdown increased 5-fluorouracil-induced apoptosis while reducing the phosphorylation of mTOR and its downstream effector P70S6K, i.e., HMGA2 acted upstream of and positively sustained AKT/mTOR/P70S6K signaling (64). This finding is directly relevant to the present study. First, it provides experimental precedent that HMGA2 functions as an upstream positive regulator of the mTOR phosphorylation cascade rather than merely a correlate of its activity, supporting the interpretation that the HMGA2-mTOR association observed here in chondrocytes may likewise reflect upstream regulation. Second, it delineates a lncRNA/HMGA2/mTOR cascade, which parallels the MIR155HG/miR-212-3p/HMGA2/mTOR axis identified in the present study, albeit in a different biological context (chemotherapy-induced apoptosis in cancer cells vs. IL-1β-induced apoptosis and autophagy dysregulation in chondrocytes).

As a transcription factor, HMGA2 may influence mTOR pathway activity through upstream components, including PI3K and Akt (65) or indirectly through intermediate mechanisms, such as regulating the expression of growth factors, including IGF2 or suppressing negative regulators (66). However, direct evidence from chromatin immunoprecipitation (ChIP) or promoter activity assays is lacking. In future studies, ChIP-qPCR should be used to identify HMGA2-binding sites in the promoters of genes involved in the mTOR pathway and HMGA2 knockdown or overexpression should be performed to identify the direct transcriptional targets within the mTOR signaling axis.

Overall, a number of notable results were obtained in the present study. Previous studies have revealed that HMGA2 is important for maintaining chondrocyte homeostasis and that its expression is generally reduced in advanced OA (32,67). However, the present results revealed that HMGA2 was upregulated in the IL-1β-induced OA-like cell model and was associated with changes in mTOR-related autophagy signaling. This discrepancy may be associated with differences in disease stage, sample composition or experimental methods. In future studies, longitudinal sampling at different stages of OA progression should be performed to further clarify the dynamic changes of HMGA2 during OA development. The present study also exhibits a number of limitations. First, there is no direct evidence that LC3-II accumulation is caused by increased autophagic flux, as it may also result from impaired autophagosome-lysosome fusion or reduced lysosomal degradation. Future studies should aim to incorporate lysosomal inhibitors, such as bafilomycin A1 or chloroquine, together with tandem fluorescent LC3 reporters (such as mRFP-GFP-LC3), to further evaluate autophagic flux. Second, the transcriptional regulatory mechanism of HMGA2 on the mTOR signaling pathway was not demonstrated. ChIP-qPCR and dual-luciferase reporter assays should be performed in future studies to determine whether HMGA2 directly binds to and regulates the promoters of mTOR pathway-related genes, including PI3K, Akt3 and mTOR. Finally, the present study was performed using an immortalized chondrocyte cell line and did not include *in vivo* experiments. Therefore, the translational relevance of the present findings requires further investigation. Future studies should aim to validate these findings in primary chondrocytes and animal models.

In summary, the present study identified the MIR155HG/miR-212-3p/HMGA2 regulatory axis associated with OA-related chondrocyte injury. MIR155HG knockdown attenuated IL-1β-induced apoptosis, ROS accumulation, mitochondrial dysfunction and extracellular matrix degradation. Rescue experiments suggested that these effects were partly mediated by miR-212-3p and associated with HMGA2 expression and mTOR-related autophagy signaling.

Acknowledgements

Not applicable.

Funding

The present study was supported by the Natural Science Foundation of Hunan Province (grant nos. 2024JJ7581, 2023JJ50426, 2024JJ6353 and 2026JJ7105), the Natural Science Fund of Changsha City (grant no. kq2403099), the Hunan Provincial Administration of Traditional Chinese Medicine (grant no. B2024062), the University-Hospital Union Fund Project of Hunan University of Chinese Medicine (grant no. 2023XYLH001) and the Hunan Provincial Health Commission Research Project (grant no. 20256210).

Availability of data and materials

The data generated in the present study may be requested from the corresponding author.

Authors' contributions

FS was responsible for conceptualization, methodology, software (including the implementation of R scripts for GEO dataset preprocessing and bioinformatics analyses) and writing the original draft. YT was responsible for data curation and validation, including cross-checking the processed datasets, analytical results and corresponding figures and tables against the original data. LC and RP were responsible for conducting the investigation. YD, XZ and RD were responsible for formal analysis. XX contributed to the study design, interpretation of experimental findings and critical revision of the manuscript for important intellectual content. SC contributed to the conception and design of the study, interpretation of the results and critical revision of the manuscript for important intellectual content. XX and SC also provided supervision, acquired funding and were responsible for project administration. FS and SC confirm

the authenticity of all the raw data. All authors have read and approved the final version of the manuscript.

Ethics approval and consent to participate

Not applicable.

Patient consent for publication

Not applicable.

Competing interests

The authors declare that they have no competing interests.

References

1. Bannuru RR, Osani MC, Vaysbrot EE, Arden NK, Bennell K, Bierma-Zeinstra SMA, Kraus VB, Lohmander LS, Abbott JH, Bhandari M, *et al*: OARSI guidelines for the non-surgical management of knee, hip, and polyarticular osteoarthritis. Osteoarthritis Cartilage 27: 1578-1589, 2019.
2. Gabner S, Ertl R, Velde K, Renner M, Jenner F, Egerbacher M and Hlavaty J: Cytokine-induced interleukin-1 receptor antagonist protein expression in genetically engineered equine mesenchymal stem cells for osteoarthritis treatment. J Gene Med 20: e3021, 2018.
3. Geng Y, Chen J, Alahdal M, Chang C, Duan L, Zhu W, Mou L, Xiong J, Wang M and Wang D: Intra-articular injection of hUC-MSCs expressing miR-140-5p induces cartilage self-repairing in the rat osteoarthritis. J Bone Miner. Metab 38: 277-288, 2020.
4. GBD 2017 Disease and Injury Incidence and Prevalence Collaborators: Global, regional, and national incidence, prevalence, and years lived with disability for 354 diseases and injuries for 195 countries and territories, 1990-2017: A systematic analysis for the global burden of disease study 2017. Lancet 392: 1789-1858, 2018.
5. Shi Y, Hu X, Cheng J, Zhang X, Zhao F, Shi W, Ren B, Yu H, Yang P, Li Z, *et al*: A small molecule promotes cartilage extracellular matrix generation and inhibits osteoarthritis development. Nat Commun 10: 1914, 2019.
6. Hasegawa A, Yonezawa T, Taniguchi N, Otabe K, Akasaki Y, Matsukawa T, Saito M, Neo M, Marmorstein LY and Lotz MK: Role of fibulin 3 in aging-related joint changes and osteoarthritis pathogenesis in human and mouse knee cartilage. Arthritis Rheumatol 69: 576-585, 2017.
7. Cao J, Liu Z, Zhang L and Li J: miR-940 regulates the inflammatory response of chondrocytes by targeting MyD88 in osteoarthritis. Mol Cell Biochem 461: 183-193, 2019.
8. Blanco FJ, Rego I and Ruiz-Romero C: The role of mitochondria in osteoarthritis. Nat Rev Rheumatol 7: 161-169, 2011.
9. Blanco FJ, Valdes AM and Rego-Pérez I: Mitochondrial DNA variation and the pathogenesis of osteoarthritis phenotypes. Nat Rev Rheumatol 14: 327-340, 2018.
10. Yang Z, Jiang W, Xiong C, Shang J, Huang Y, Zhou X and Zhang S: Calcipotriol suppresses GPX4-mediated ferroptosis in OA chondrocytes by blocking the TGF-β1 pathway. Cytokine 171: 156382, 2023.
11. Pelletier JP, Raynauld JP, Dorais M, Bessette L, Dokoupilova E, Morin F, Pavelka K, Paiement P and Martel-Pelletier J; DISSCO Trial Investigator Group: An international, multicentre, double-blind, randomized study (DISSCO): Effect of diacerein vs celecoxib on symptoms in knee osteoarthritis. Rheumatology (Oxford) 59: 3858-3868, 2020.
12. Zeng C, Zhang W, Doherty M, Persson MSM, Mallen C, Swain S, Li X, Wei J, Lei G and Zhang Y: Initial analgesic prescriptions for osteoarthritis in the United Kingdom, 2000-2016. Rheumatology (Oxford) 60: 147-159, 2021.
13. Elmore S: Apoptosis: A review of programmed cell death. Toxicol Pathol 35: 495-516, 2007.
14. Xu X, Lai Y and Hua ZC: Apoptosis and apoptotic body: Disease message and therapeutic target potentials. Biosci Rep 39: BSR20180992, 2019.
15. Wang Y, Xu Y and Zhu C: The role of autophagy in childhood central nervous system tumors. Curr Treat Options Oncol 23: 1535-1547, 2022.
16. Xilouri M and Stefanis L: Autophagy in the central nervous system: Implications for neurodegenerative disorders. CNS Neurol Disord Drug Targets 9: 701-719, 2010.
17. Maiuri MC, Zalckvar E, Kimchi A and Kroemer G: Self-eating and self-killing: Crosstalk between autophagy and apoptosis. Nat Rev Mol Cell Biol 8: 741-752, 2007.
18. Feng K, Chen H and Xu C: Chondro-protective effects of celastrol on osteoarthritis through autophagy activation and NF-κB signaling pathway inhibition. Inflamm Res 69: 385-400, 2020.
19. Sun K, Luo J, Guo J, Yao X, Jing X and Guo F: The PI3K/AKT/mTOR signaling pathway in osteoarthritis: A narrative review. Osteoarthritis Cartilage 28: 400-409, 2020.
20. Zheng W, Li X, Liu D, Li J, Yang S, Gao Z, Wang Z, Yokota H and Zhang P: Mechanical loading mitigates osteoarthritis symptoms by regulating endoplasmic reticulum stress and autophagy. FASEB J 33: 4077-4088, 2019.
21. Zheng G, Zhan Y, Li X, Pan Z, Zheng F, Zhang Z, Zhou Y, Wu Y, Wang X, Gao W, *et al*: TFEB, a potential therapeutic target for osteoarthritis via autophagy regulation. Cell Death Dis 9: 858, 2018.
22. Xu K, He Y, Moqbel SAA, Zhou X, Wu L and Bao J: SIRT3 ameliorates osteoarthritis via regulating chondrocyte autophagy and apoptosis through the PI3K/Akt/mTOR pathway. Int J Biol Macromol 175: 351-360, 2021.
23. Clark BS and Blackshaw S: Understanding the role of lncRNAs in nervous system development. Adv Exp Med Biol 1008: 253-282, 2017.
24. Herman AB, Tsitsipatis D and Gorospe M: Integrated lncRNA function upon genomic and epigenomic regulation. Mol Cell 82: 2252-2266, 2022.
25. Diman A and Decottignies A: Genomic origin and nuclear localization of TERRA telomeric repeat-containing RNA: From Darkness to Dawn. FEBS J 285: 1389-1398, 2018.
26. Huang W, Huang F, Lei Z and Luo H: LncRNA SNHG11 promotes proliferation, migration, apoptosis, and autophagy by regulating hsa-miR-184/AGO2 in HCC. Onco Targets Ther 13: 413-421, 2020.
27. Zhou Q, Liu J, Xin L, Fang Y, Qi Y and Hu Y: Identification of characteristic lncRNA molecular markers in osteoarthritis by integrating GEO database and machine learning strategies and experimental validation. Sichuan Da Xue Xue Bao Yi Xue Ban 54: 899-907, 2023 (In Chinese).
28. Montagne K, Furukawa KS, Taninaka Y, Ngao B and Ushida T: Modulation of the long non-coding RNA Mir155hg by high, but not moderate, hydrostatic pressure in cartilage precursor cells. PLoS One 17: e0275682, 2022.
29. Liu R, Ye J and Huang S: LncRNA MIR155HG suppresses cell apoptosis by activating autophagy via miR-7036b-3p/GPNMB axis and AMPK/mTOR signaling in spinal cord injury. Noncoding RNA Res 15: 1-17, 2025.
30. Ma N, Tie C, Yu B, Zhang W and Wan J: Identifying lncRNA-miRNA-mRNA networks to investigate Alzheimer's disease pathogenesis and therapy strategy. Aging (Albany NY) 12: 2897-2920, 2020.
31. Dutta A, Hutchison RE and Mohi G: Hmga2 promotes the development of myelofibrosis in $Jak2^{V617F}$ knockin mice by enhancing TGF-β1 and Cxcl12 pathways. Blood 130: 920-932, 2017.
32. Jouan Y, Bouchemla Z, Bardèche-Trystram B, Sana J, Andrique C, Ea HK, Richette P, Latourte A, Cohen-Solal M and Hay E: Lin28a induces SOX9 and chondrocyte reprogramming via HMGA2 and blunts cartilage loss in mice. Sci Adv 8: eabn3106, 2022.
33. Cheng C, Yao H, Li H, Liu J, Liu Z, Wu Y, Zhu L, Hu H, Fang Z and Wu L: Blockade of the deubiquitinating enzyme USP48 degrades oncogenic HMGA2 and inhibits colorectal cancer invasion and metastasis. Acta Pharm Sin B 14: 1624-1643, 2024.
34. Li Y, Qiang W, Griffin BB, Gao T, Chakravarti D, Bulun S, Kim JJ and Wei JJ: HMGA2-mediated tumorigenesis through angiogenesis in leiomyoma. Fertil Steril 114: 1085-1096, 2020.
35. Zhu W, Yu J, Qiu S, Liu H, Wang Y, Xu X, Shao L, Zhu L, Jiao Y, Liu F and Zhu X: MiR-let-7a regulates anti-citrullinated protein antibody-induced macrophage activation and correlates with the development of experimental rheumatoid arthritis. Int Immunopharmacol 51: 40-46, 2017.
36. Lv W, Yuan J, Ruan Z, Dou YN, Zhang H, Fei X, Chen L, Zhang Z, Yang K, Wu X, *et al*: Single-cell transcriptome analysis reveals that Hmga2 regulates neuroinflammation and retinal function by modulating Müller cell autophagy through PI3K/AKT signaling following MCAO-induced retinal ischemia. Adv Sci (Weinh) 12: e02534, 2025.

37. Liu L, Zhang W, Liu T, Tan Y, Chen C, Zhao J, Geng H and Ma C: The physiological metabolite α-ketoglutarate ameliorates osteoarthritis by regulating mitophagy and oxidative stress. Redox Biol 62: 102663, 2023.
38. Fisch KM, Gamini R, Alvarez-Garcia O, Akagi R, Saito M, Muramatsu Y, Sasho T, Koziol JA, Su AI and Lotz MK: Identification of transcription factors responsible for dysregulated networks in human osteoarthritis cartilage by global gene expression analysis. Osteoarthritis Cartilage 26: 1531-1538, 2018.
39. Chou CH, Wu CC, Song IW, Chuang HP, Lu LS, Chang JH, Kuo SY, Lee CH, Wu JY, Chen YT, *et al*: Genome-wide expression profiles of subchondral bone in osteoarthritis. Arthritis Res Ther 15: R190, 2013.
40. Ritchie ME, Phipson B, Wu D, Hu Y, Law CW, Shi W and Smyth GK: limma powers differential expression analyses for RNA-sequencing and microarray studies. Nucleic Acids Res 43: e47, 2015.
41. Eisen MB, Spellman PT, Brown PO and Botstein D: Cluster analysis and display of genome-wide expression patterns. Proc Natl Acad Sci USA 95: 14863-14868, 1998.
42. Ito K and Murphy D: Application of ggplot2 to pharmacometric graphics. CPT Pharmacometrics Syst Pharmacol 2: e79, 2013.
43. Wu T, Hu E, Xu S, Chen M, Guo P, Dai Z, Feng T, Zhou L, Tang W, Zhan L, *et al*: clusterProfiler 4.0: A universal enrichment tool for interpreting omics data. Innovation (Camb) 2: 100141, 2021.
44. Hu X, Wang J, Ju Y, Zhang X, Qimanguli W, Li C, Yue L, Tuohetaerbaike B, Li Y, Wen H, *et al*: Combining metabolome and clinical indicators with machine learning provides some promising diagnostic markers to precisely detect smear-positive/negative pulmonary tuberculosis. BMC Infect Dis 22: 707, 2022.
45. Livak KJ and Schmittgen TD: Analysis of relative gene expression data using real-time quantitative PCR and the 2(-Delta Delta C(T)) method. Methods 25: 402-408, 2001.
46. John B, Enright AJ, Aravin A, Tuschl T, Sander C and Marks DS: Human MicroRNA targets. PLoS Biol 2: e363, 2004.
47. Cao H, Yang P, Liu J, Shao Y, Li H, Lai P, Wang H, Liu A, Guo B, Tang Y, *et al*: MYL3 protects chondrocytes from senescence by inhibiting clathrin-mediated endocytosis and activating of Notch signaling. Nat Commun 14: 6190, 2023.
48. Guilak F, Nims RJ, Dicks A, Wu CL and Meulenbelt I: Osteoarthritis as a disease of the cartilage pericellular matrix. Matrix Biol 71-72: 40-50, 2018.
49. Nedunchezhiyan U, Varughese I, Sun AR, Wu X, Crawford R and Prasadam I: Obesity, inflammation, and immune system in osteoarthritis. Front Immunol 13: 907750, 2022.
50. Picard M, Wallace DC and Burelle Y: The rise of mitochondria in medicine. Mitochondrion 30: 105-116, 2016.
51. Court AC, Vega-Letter AM, Parra-Crisóstomo E, Velarde F, García C, Ortloff A, Vernal R, Pradenas C, Luz-Crawford P, Khoury M and Figueroa FE: Mitochondrial transfer balances cell redox, energy and metabolic homeostasis in the osteoarthritic chondrocyte preserving cartilage integrity. Theranostics 14: 6471-6486, 2024.
52. Collins JA, Wood ST, Nelson KJ, Rowe MA, Carlson CS, Chubinskaya S, Poole LB, Furdui CM and Loeser RF: Oxidative stress promotes peroxiredoxin hyperoxidation and attenuates pro-survival signaling in aging chondrocytes. J Biol Chem 291: 6641-6654, 2016.
53. Jiang Z, Qi G, Lu W, Wang H, Li D, Chen W, Ding L, Yang X, Yuan H and Zeng Q: Omaveloxolone inhibits IL-1β-induced chondrocyte apoptosis through the Nrf2/ARE and NF-κB signalling pathways in vitro and attenuates osteoarthritis in vivo. Front Pharmacol 13: 952950, 2022.
54. Vergroesen PP, Kingma I, Emanuel KS, Hoogendoorn RJ, Welting TJ, van Royen BJ, van Dieën JH and Smit TH: Mechanics and biology in intervertebral disc degeneration: A vicious circle. Osteoarthritis Cartilage 23: 1057-1070, 2015.
55. Hashimoto K, Otero M, Imagawa K, de Andrés MC, Coico JM, Roach HI, Oreffo ROC, Marcu KB and Goldring MB: Regulated transcription of human matrix metalloproteinase 13 (MMP13) and interleukin-1β (IL1B) genes in chondrocytes depends on methylation of specific proximal promoter CpG sites. J Biol Chem 288: 10061-10072, 2013.
56. Bao J, Chen Z, Xu L, Wu L and Xiong Y: Rapamycin protects chondrocytes against IL-18-induced apoptosis and ameliorates rat osteoarthritis. Aging (Albany NY) 12: 5152-5167, 2020.
57. Nakatogawa H: Mechanisms governing autophagosome biogenesis. Nat Rev Mol Cell Biol 21: 439-458, 2020.
58. Li J, Jiang M, Yu Z, Xiong C, Pan J, Cai Z, Xu N, Zhou X, Huang Y and Yang Z: Artemisinin relieves osteoarthritis by activating mitochondrial autophagy through reducing TNFSF11 expression and inhibiting PI3K/AKT/mTOR signaling in cartilage. Cell Mol Biol Lett 27: 62, 2022.
59. Guo P, Li H, Wang X, Li X and Li X: PG545 prevents osteoarthritis development by regulating PI3K/AKT/mTOR signaling and activating chondrocyte autophagy. Pharmacology 108: 576-588, 2023.
60. Wang J and Li J: LncRNA MIR155HG functions as a ceRNA for inhibition of lung adenocarcinoma growth and prediction of prognosis. Arch Med Sci 20: 539-556, 2021.
61. Zhong J, He C, Xu F, Xu X, Liu L, Xu M, Guo Z, Wang Y, Liao J and Li Y: Lupeol inhibits osteosarcoma progression by up-regulation of HMGA2 via regulating miR-212-3p. J Orthop Surg Res 15: 374, 2020.
62. Dai J, Hu Z, Zeng F, Gong X, Tang H, Deng J, Li J and Dong S: Osteoclast-derived exosomal miR-212-3p suppressed the anabolism and accelerated the catabolism of chondrocytes in osteoarthritis by targeting TGF-β1/Smad2 signaling. Arch Biochem Biophys 751: 109827, 2024.
63. Chen W, Ma X, Zhang P, Li Q, Liang X and Liu J: MiR-212-3p inhibits LPS-induced inflammatory response through targeting HMGB1 in murine macrophages. Exp Cell Res 350: 318-326, 2017.
64. Bai L, Dong K, Tong D, Shi X, Wei S and Cai Y: lncRNA HIT000218960 enhances resistance to 5-fluorouracil by promoting HMGA2 and activating the AKT/mTOR/P70S6K pathway in gastric cancer cells. Exp Ther Med 24: 527, 2022.
65. Mansoori B, Mohammadi A, Ditzel HJ, Duijf PHG, Khaze V, Gjerstorff MF and Baradaran B: HMGA2 as a critical regulator in cancer development. Genes (Basel) 12: 269, 2021.
66. Carrabotta M, Laginestra MA, Durante G, Mancarella C, Landuzzi L, Parra A, Ruzzi F, Toracchio L, De Feo A, Giusti V, *et al*: Integrated molecular characterization of patient-derived models reveals therapeutic strategies for treating CIC-DUX4 sarcoma. Cancer Res 82: 708-720, 2022.
67. Bao C, Zhu S, Pang D, Yang M, Huang J, Wang F, Hou Y, Wang X, Feng Y, Yang H, *et al*: Hexokinase 2 suppression alleviates the catabolic properties in osteoarthritis via HMGA2 and contributes to pulsed electromagnetic field-mediated cartilage protection. Int J Biol Sci 21: 1459-1477, 2025.

Copyright © 2026 Shen et al. This work is licensed under a Creative Commons Attribution-NonCommercial-NoDerivatives 4.0 International (CC BY-NC-ND 4.0) License.